DIAGNOSTICS OF FILAMENT-ASSISTED DIAMOND GROWTH CHEMISTRY

F.G. Celii,* P.E. Pehrsson and J.E. Butler
Chemistry Division, Naval Research Laboratory, Washington, D.C. 20375-5000

ABSTRACT

The use of in-situ optical diagnostics for probing the gas phase in the chemical vapor deposition (CVD) of diamond is described. Radical species (H and CH_3) as well as stable molecules (CH_4, C_2H_2, C_2H_4) have been detected with these techniques. We summarize here the results of resonance-enhanced multiphoton ionization (REMPI) studies and infrared diode laser absorption measurements made under filament-assisted diamond CVD conditions. The concentrations of two potential carbon-transport species, CH_3 and C_2H_2, both increased as a function of the initial CH_4/H_2 fraction (F_0), whereas the H atom concentration decreased with increasing F_0. In conjunction with known diamond film growth results, we interpret these observations as evidence for the *surface* role of atomic hydrogen in the diamond growth mechanism.

INTRODUCTION

Diamond has outstanding material properties, such as extreme hardness and high thermal conductivity.[1] The same properties make diamond exceedingly difficult to modify (*e.g.,* by machining or doping). Modification could in principle be more easily accomplished during vapor phase deposition, so the prospect of CVD-synthesized diamond is of great practical importance. Various diamond CVD techniques have already been demonstrated,[2] but development of improved deposition methods will be hindered without an understanding of the diamond formation mechanism. The fact that CVD diamond growth proceeds under temperature and pressure conditions at which graphite is the stable carbon form indicates that a delicate balance is needed for growth. Diamond deposition might be further manipulated once the mechanisms leading to this balance are understood.

Much insightful work has led to an empirical understanding of the diamond growth environment. Supersaturation of atomic hydrogen is crucial[3] for diamond deposition, although it's exact role in the growth process is not clear. The postulated carbon-transport species have generally been hydrocarbon pyrolysis products, notably CH_3,[3,4] CH and atomic carbon.[5] Other proposed mechanisms[6-8] find low calculated activation barriers based on C_2H_2[6], or CH_3^+/CH_3[7] as the active growth species. Only recently have in-situ gas phase measurements[9-11] been performed enabling testing of these hypotheses. We report here on determinations of the filament-assisted diamond growth chemistry made through the use of spectroscopic probes.

EXPERIMENTAL

The chamber used for both the deposition of diamond films and the infrared absorption measurements was described previously.[9] Briefly, a tungsten filament was suspended 1.5 cm above a substrate (e.g., Si wafers or Ni foil) and mounted in the center of a stainless steel 6-way cross. Typical growth conditions included a slow flow (100 sccm) of <1.0% CH_4 in H_2 at 25 Torr total pressure, and a tungsten filament temperature (T_{fil}) of ~2000 C (measured with a 2-color pyrometer). The substrate, heated by radiation and convection, was maintained

in a temperature range necessary for diamond growth ($\sim$900 C).

Mirrors were mounted inside the chamber to provide a multi-pass geometry for the infrared absorption measurements. The diode laser beam passed $\sim$20 times through the chamber, including a region located few mm above the substrate, before being focussed onto an infrared detector. Molecular species within the pathlength resonantly absorb the tunable IR light and are detected by the concommitant power loss at the detector. For the REMPI experiments, a focussed dye laser beam (1-15 mJ/pulse, $\Delta\nu \sim 0.2$ cm^{-1}), made 1 or 2 passes through the chamber. The substrate holder was biased ($\sim$150V) to provide efficient collection of photoelectrons (generated by the MPI process) at a Pt probe wire inserted 2-4 mm above the subtrate and 1-2 mm from the focal volume of the laser.[11]

RESULTS AND DISCUSSION

The films deposited in this chamber were analyzed with a variety of techniques which definitively established diamond deposition: SEM micrographs showed facetted crystallites, whether isolated or in polycrystalline films; Raman spectra exhibited an intense, sharp 1332 cm^{-1} band, with little evidence for graphitic or amorphous carbon; small-spot Auger electron spectroscopy detected only carbon, with a lineshape similar to that of natural diamond; x-ray diffraction spectra yielded a diamond lattice constant.[9] All spectroscopic investigations were conducted under similar diamond growth conditions, although deposits were not always analyzed.

With $F_0=$ 0.5% and $T_{fil}=$ 2000 C, the following gas phase species concentrations present during diamond CVD were determined from infrared absorption measurements: CH_4, $8 \pm 3 \times 10^{14}$cm^{-3} ($\sim$50 mTorr @ 300 C); CH_3, $2 \bullet 1.5 \times 10^{12}$; C_2H_4, $6 \pm 2 \times 10^{12}$; and C_2H_2, $2 \pm 1 \times 10^{14}$. No absorption lines due to C_2H_6 or stable C_3H_y species were found. Experiments to follow the concentration of these species as a function of various growth parameters are currently in progress.

The IR observations can be qualitatively understood by consideration of the initial gas mixture at elevated temperatures (1300<T<2500 C), where C_2H_2 is the thermodynamically-favored carbon-containing molecule. Various hydrocarbon fuels would be predicted to generate similar species by this technique. Detection of transient species (i.e., C_2, CH and C_3), which are predicted by the thermodynamic model to be present in detectable concentrations, was attempted using laser-excited fluorescence (LEF), but only C_3 was tentatively identified. The absence of ground state C_2 and CH in detectable concentration indicates that while these species may be produced at the hot filament, they are consumed by reactions occuring at lower temperature during transport to the surface. Both CH and C_2 have been detected from their excited-state optical emission spectrum during plasma-assisted diamond growth, but were not present in sufficient quantity to account for the observed rate of filament-assisted diamond growth. The observed concentrations of CH_4, CH_3, C_2H_2 or C_2H_4 could account for the diamond deposition rate.

Using in-situ mass spectrometric analysis, Harris, et al.[10] also observed significant conversion of CH_4 to C_2H_2 in a filament-assisted diamond CVD chamber. The radical species concentrations predicted by their kinetic modeling study are in agreement with our observations. It was concluded that the probable carbon-transport species in this system are CH_3, C_2H_2, CH_4 and C_2H_4, with preference given to CH_3 and C_2H_2 based on reactivity.[10]

The 2+1 REMPI band at 333.5 nm[12] was employed for in-situ detection of CH_3. The spatial resolution of the REMPI detection provides relative concentration measurements in a

479

volume directly above the growth surface. In Fig. 1, the C_2H_2 concentration derived from the IR absorption measurements is compared with the CH_3 REMPI signal. Note that for $F_0 = 0.5\%$ the average CH_3 concentration through the diode beam path is about 2 orders of magnitude lower than that of C_2H_2. Both species concentrations increased for increased F_0, with C_2H_2 growing at perhaps a faster rate.

To monitor the concentration of atomic hydrogen, the REMPI technique was employed, with specific detection provided by the 3+1 resonant transition at 364.7 nm.[13] An interference effect was observed in the single pass (travelling wave–TW) geometry due to the generation of third harmonic light, manifested by the absence of the resonant REMPI feature at 364.68 nm. The resonant REMPI peak was obtained using standing-wave (SW) excitation (a spherical mirror re-focussed the UV beam back along the optical axis). The observations are consistent with theoretical predictions[14] and experimental verifications (in rare gases)[15] of an interference effect between odd harmonics of the laser field (in this case, the first and third harmonics, at 364.7 nm and 121.6 nm, respectively).

The hydrogen atom concentration can be monitored using the intensity of the resonant REMPI signal from the SW excitation geometry. The T_{fil} dependence of the 365.68 nm feature for pure H_2 (Fig. 2(a)) agrees with the thermodynamics for H_2 dissociation. The signal attenuation at $F_0 = 0.5\%$ and 1.0% reflects a loss in H atom flux in a probed volume located 8 mm from the filament, probably due to gas-phase reactions. The $F_0 = 3\%$ curve (Fig. 2(d)) suggests a poisoning of the filament surface resulting in severely reduced H atom concentration for T_{fil} less than 2200 C. The poisoning, perhaps related to a tungsten carbide phase, might be avoided with the use of alternate filament materials, such as rhenium.

For CH_4 in H_2, it has been shown that $F_0 < 1\%$ is necessary for growth of reasonable purity diamond. The diminished H atom flux for $F_0 > 1\%$ correlates with observations[16,17] of increased deposition of graphitic and amorphous carbon under these conditions; however, the measured concentration of CH_3 and C_2H_2 both increase with F_0, even for $F_0 > 1\%$ (Fig. 1). We interpret these results as suggesting that the dominant role played by atomic hydrogen in diamond CVD is surface-related (e.g., dangling surface bond termination, preparation of active surface sites, and/or preferential etching of non-diamond forms of carbon), rather than generation of gas-phase intermediates.

SUMMARY

Our present model of the filament-assisted gas phase environment, in concert with that of Harris, et al.,[10] is one in which thermodynamically-favored species (e.g., C_2H_2, CH_3) are formed at high temperature near the filament, followed by depletion of the more reactive species during transport to the diamond growth surface. The carbon-transport, or growth, species for this system may be CH_4, C_2H_4, CH_3 or C_2H_2, but CH and C_2 do not appear to play a significant role in carbon deposition. Some aspects of polycrystalline diamond film growth correlate with hydrogen atom concentration, and we conclude that the interaction of hydrogen atom with the growing diamond surface is important, while the role of H atoms in gas phase chemistry appear to be less important.

ACKNOWLEDGEMENTS

REFERENCES

* National Research Council Postdoctoral Fellow.

1. Field, J. E. *"The Properties of Diamond,"* Academic Press, New York, 1979.

2. See, for example: Angus, J. C., Will, H. A. and Stanko, W. S. *J. Appl. Phys.,* 1968 39, 2915; Spitsn, B. V., Bouilov, L. L. and Derjaguin, B. V. *J. Cryst. Growth,* 1981, 52, 219; Kamo, M., Sato, Y., Matsumoto, S. and Setaka, N. *J. Cryst. Growth,* 1983, 62, 642; Sawabe A. and Inzuka, T. *Appl. Phys. Lett.,* 1985, 46, 146; Kasi, S., Kang, H. and Rabalais, J. W. *Phys. Rev. Lett.,* 1987, 59, 75.

3. For excellent reviews, see: DeVries, R. C. *Ann. Rev. Mater. Sci.,* 1987, 17, 161; Angus, J. C. and Hayman, C. C. *Science,* 1988, 241, 913; Badzian, A. R. and DeVries, R. C. *Mat. Res. Bull.,* 1988, 23, 385; Derjaguin, B. V. and Fedoseev, D. B. *Sci. Amer.,* 1968, 233 (5) 102.

4. Hirose, Y. and Terasawa, Y. *Jap. J. Appl. Phys.,* 1986, 25, L519.

5. Matsumoto, S., Sato, Y., Tsutsumi, M. and Setaka, N. *J. Mater. Sci.,* 1982, 17, 3106.

6. Frenklach, M. and Spear, K. E. *J. Mater. Res.,* 1988, 3, 133; Huang, D., Frenklach M. and Maroncelli, M. *J. Phys. Chem.,* 1988, 92, 6379.

7. Tsuda, M., Nadajima, M. and Oikawa, S. *J. Amer. Chem. Soc.,* 1986, 108, 5780.

8. Sommer, M., Mui, K. and Smith, F. W. *Appl. Phys. Lett.,* in press.

9. Celii, F. G., Pehrsson, P. E., Wang, H. -t. and Butler, J. E. *Appl. Phys. Lett.,* 1988, 52, 2043.

10. Harris, S. J., Weiner, A. M. and Perry, T. A. *Appl. Phys. Lett.,* 1988, 53, 1605.

11. Celii, F. G. and Butler, J. E. *Appl. Phys. Lett.,* submitted for publication.

12. Hudgens, J. W., DiGuiseppe, T. G. and Lin, M. C. *J. Chem. Phys.,* 1983, 79, 571.

13. Tjossem, P. J. H. and Cool, T. A. *Chem. Phys. Lett.,* 1983, 100, 479.

14. Jackson, D. J. and Wynne, J. J. *Phys. Rev. Lett.,* 1982, 49, 543; Payne, M. G., Garrett, W. R. and Ferrell, W. R. *Phys. Rev. A,* 1986, 34, 1143.

15. Glownia, J. H. and Sander, R. K. *Phys. Rev. Lett.,* 1982, 49, 21.

16. Singh, B., Arie, Y., Levine, A. W. and Mesker, O. R. *Appl. Phys. Lett.,* 1988, 52, 451.

17. Zhu, W., Randall, C., Badzian, A. R. and Messier, R., to be published.
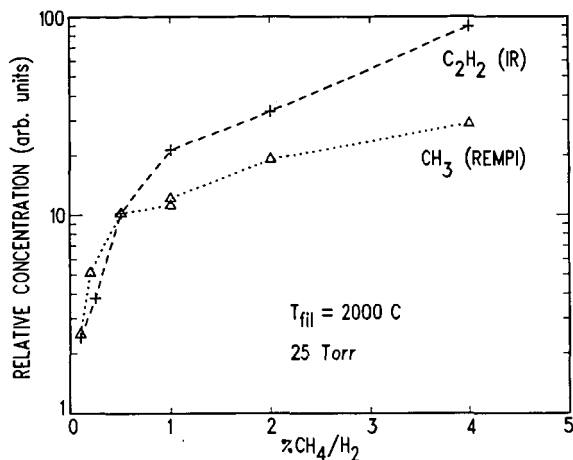
Figure 1: Relative concentrations of C_2H_2 (crosses, from infrared absorption), and CH_3 (triangles, REMPI data) *vs.* F_0. The IR measurements were not spatially resolved.
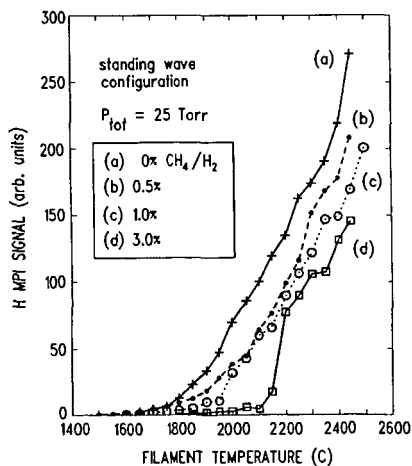

Figure 2: Relative H atom concentrations *vs.* filament temperature. The lines are merely to connect data points for each inital F_0 value, given in the figure. All data are for a filament-probe separation of 8 mm.

Ultrasensitive Absorption Spectroscopy
by Intracavity Laser Techniques

George H. Atkinson and James J. O'Brien
Department of Chemistry and Optical Sciences Center
University of Arizona, Tucson, Arizona 85721

INTRODUCTION

Diagnostic techniques which can be used to monitor spectroscopically the gas phase during the chemical vapor deposition (CVD) of material on a substrate are of significant value both in the analysis of reaction mechanisms and in the real time control of deposition conditions. The in situ detection of gas phase intermediates during CVD is of special importance in obtaining a realistic understanding of the mechanism(s) underlying the preparation of a specific deposited material. These in situ diagnostic measurements also can be utilized to optimized processing conditions.

Laser induced fluorescence (LIF) has often been used to monitor reaction intermediates because of its high sensitivity for detecting gas phase molecules. Many chemical conditions which facilitate CVD, however, are not well suited for LIF spectroscopy due to highly reactive environments and pressure conditions which quench emission yields or because of the large amounts of background emission created by the dissociative processes, e.g.; during plasma discharge. By contrast, absorption spectroscopy has long been recognized as a widely applicable technique which can be readily utilized in chemical, pressure, and radiation conditions not conducive to LIF detection. The major limitation is sensitivity which in conventional absorption spectroscopy has prevented its application to monitoring low concentrations of molecules and radical concentrations.

Recently, the limited detection sensitivity of absorption spectroscopy has been addressed through the development of intracavity laser spectroscopy (ILS) [1,2]. ILS techniques have been used in a variety of instrumental configurations to demonstrate enhanced detection sensitivities for absorption measurements of many orders of magnitude relative to conventional absorption spectroscopy [1,2]. The enhanced sensitivity derives from the competition between the gain in the laser medium and the wavelength-dependent losses within the laser resonator. By placing the species of interest inside the optical resonator cavity of a longitudinally multimode laser, the absorption spectrum of the intracavity atomic or molecular species is superimposed on the wavelength-dispersed spectrum of the laser output.

EXPERIMENTAL

The ILS laser system is shown schematically in Figure 1. A modified dye laser (Coherent 590) is pumped by an argon ion laser (Coherent I-53-8 or Coherent I-53-18). The pumping radiation is attenuated as a function of time (33 Hz) by passing it through an acousto-optic modulator (AOM1). AOM1 diverts enough pump power to prevent the dye laser from reaching threshold conditions. When AOM1 is switched off, the pump laser brings the dye laser rapidly above threshold (~0.15 μs). The dye laser output passes through a second acousto-

optic modulator (AOM2) which deflects part of the dye laser output to the spectrometer. The wavelength-dispersed radiation exiting the spectrometer is focused onto the face of an intensified vidicon camera. Such multichannel detection makes it feasible to monitor substantial portions of the rovibronic absorption spectrum of the intracavity species in real time.

The period of time during which the dye laser operates above threshold and AOM2 remains open determines the generation time, t_g, of the ILS laser system [3]. It has been shown that the intracavity absorption obeys a Beer-Lambert relationship with the equivalent pathlength of absorption, L_{eq}, given by $L_{eq} = R.t_g.c$ where R is the ratio of the pathlength of the laser through the intracavity absorber to the length of the laser resonator cavity and c is the velocity of light. For the results presented here, L_{eq} was in the range of 3 - 50 km.

The wavelength of the ILS dye laser is controlled by angle tuning an intracavity pellicle. The spectral bandwidth of the dye laser is 0.8 nm (22 cm^{-1}) and the overall spectral resolution of the detection system is about 95000 (0.18 cm^{-1}). The spectra presented here are a composite of a number of individual spectra obtained from overlapping wavelength regions.

Contained within the 1 m long cavity of the dye laser is the sample cell. It is equipped with 0.5 inch thick, fused-silica windows positioned at Brewster's angle. During the CVD process, these windows are continuously flushed with hydrogen or argon to prevent contamination by any particulate products of the decomposition which would render the cell windows opaque to the transmission of the laser radiation. The sample cell is modular in design consisting of sections of quartz tubing joined together using stainless steel fittings (Cajon Ultra-Torr). Decomposition of the source material in the intracavity cell is accomplished by (1) a microwave discharge in an Everson-Broida cavity operated at ~100 W and in a geometry concentric with the laser axis or (2) pyrolysis in an 1500 W tube furnace surrounding the central 6" section of the cell. The various gases used are introduced into the cell by stainless steel handling systems which include flowmeters and mass flow controllers.

In order to examine resulting deposited films, 1/4" x 1/2" sections of oxidized (~1 μm thick) silicon wafer are placed inside the decomposition zone of the intracavity CVD cell. The surface composition of the films prepared by the CVD processes are examined by XPS analysis.

RESULTS AND DISCUSSION

We have previously reported the ILS detection of silylene (SiH_2) in the microwave discharge decomposition of silane in argon [4,5]. Electronically excited argon and H_2 species are observed also under some of these conditions. Different concentrations of SiH_2 are observed by ILS in the microwave discharge decomposition of phenylsilane, ethylsilane and ethyltrichlorosilane under similar experimental conditions. Since several studies [6] have indicated that SiH_2 is a dominant precursor to Si and α-Si-H deposition, its detection is of special importance in examining source materials for the preparation of silicon.

Figure 2 shows a section of the ILS spectrum observed during the pyrolysis of silane at 750 °C and with a total pressure of 6.2 Torr in a 1:1 mix with H_2. The wavelength region is within the (0,3,0)-(0,0,0) vibronic band in the A←X transition of SiH_2. Almost all the absorption features in this spectrum are due to known transitions of SiH_2. Spectra in this wavelength region also have been obtained during the pyrolysis of a number of organosilanes. Different relative intensities of SiH_2 absorption transitions are observed under similar pyrolysis conditions. For example, more intense SiH_2 absorptions can be observed in the pyrolysis of ethylsilane than in the pyrolysis of silane.

A primary obstacle to the use of organosilanes for the CVD of silicon is the seemingly inevitable incorporation of carbon in the resulting silicon films. It is thought that carbon deposition under these conditions occurs via a polymeric process [7]. As a consequence, the radical C_2 is a possible gas phase precursor to carbon incorporation in the films. Figure 3 shows a section of the ILS spectrum obtained of the microwave discharge decomposition of 0.1 Torr of acetylene in 0.8 Torr of argon in the region of the 0-1 band head of the C_2 Swan system [8].

Both the SiH_2 and C_2 ILS absorption spectra are recorded under real time, *in situ* CVD conditions which produce deposited films. In the case of pyrolysis of silane (Figure 2), XPS analysis of the deposited material show that it is essentially pure crystalline silicon. The XPS analysis of the films produced during the plasma discharge of acetylene demonstrate a pure carbon composition. The short (1-5 sec) accumulation times for these ILS data facilitate the control and optimization of CVD conditions through diagnostic measurements of gas phase species.

Stable molecules also can be monitored directly by ILS through either allowed (e.g., visible electronic transitions of NO_2 [9,10]) or forbidden absorptions (e.g., vibrational overtone transitions in the ground electronic state of CH_4 [11,12]). Although the latter overtone transitions are of particular interest in astronomical spectroscopy [13], they also may be used in absorption diagnostics via ILS. Figure 4 presents the overtone absorption spectrum of CH_4 recorded by ILS near 682 nm for a room temperature sample (610 Torr). The absorption strength of this line has been measured by ILS [11,12] as have collisional broadening parameters [12].

The diagnostic capabilities of ILS in CVD have one additional experimental characteristic which can be of significant practical advantage. Since the spectral information is contained on the laser beam which exits the dye laser cavity, the ILS data can be transmitted over optical fibers. It has recently been demonstrated that absorption data recorded by ILS can transverse an optical fiber without significant distortion [14].

REFERENCES

1. G.H. Atkinson, in Advances in Chemical Reaction Dynamics (P.M. Rentzepis and C.Capellos, eds.) (1986) 207.
2. J.J. O'Brien, N. Goldstein, and G.H. Atkinson in Laser Applications in Chemical Dynamics (M.A. El-Sayed, ed.) (1987) 87-95.
3. F. Stoeckel and G.H. Atkinson, Appl. Optics, 24 (1985) 3591.
4. J.J. O'Brien and G.H. Atkinson, Chem. Phys. Lett., 130 (1986) 321.

5. J.J. O'Brien and G.H. Atkinson, J. Phys. Chem, **92** (1988) 5782.
6. For example, B.A. Scott, R.M. Plecenik and E.E. Simonyi, Appl. Phys. Letters **39** (1981) 73.
7. J.S. Francisco, S.A. Joyce, J.I. Steinfeld and F. Walsh, J. Phys. Chem. **88** (1984) 3098.
8. J. G. Phillips, Ap. J. **108** (1948) 434.
9. G.H. Atkinson, T. Heimlich and M.W. Schuyler, J. Chem. Phys. **66** (1977) 5002.
10. N. Goldstein, T.L. Brack and G.H. Atkinson, Chem. Phys. Lett. **116** (1985) 223.
11. E.N. Atonov, E.B. Berik and V.G. Koloshnikov, J. Quant. Spectrosc. Radiat. Transfer **22** (1979) 45.
12. J.J. O'Brien, P. Cvijin Vujkovic, K. Wells, D. Hunten, J. Lunine, and G.H. Atkinson (unpublished results).
13. L.P. Giver, J. Quant. Spectrosc. Radiat. Transfer **19** (1978) 311.
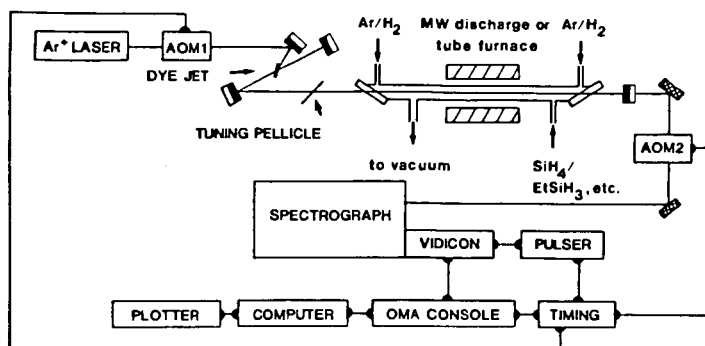14. J.J. O'Brien, W. Torruellas and G.H. Atkinson, Appl. Optics. **26** (1987) 4563.

Figure 1. Instrumentation used for intracavity laser spectroscopy of gaseous species produced in the pyrolytic and/or microwave discharge decomposition of source compounds for SiH_2.
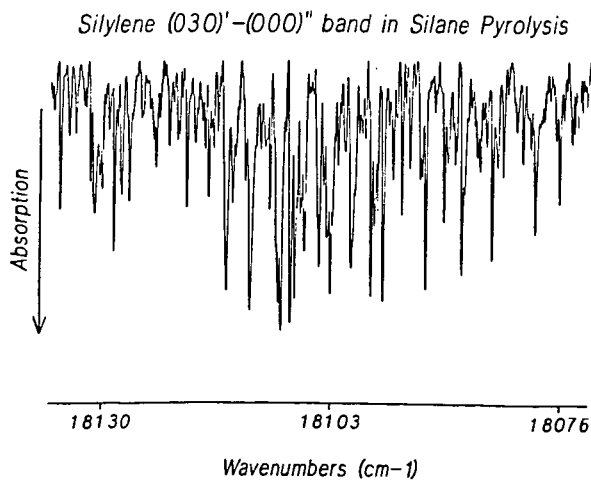
Silylene (030)'–(000)" band in Silane Pyrolysis

Figure 2. ILS spectrum for the pyrolysis of 52% silane in H_2 at 8.5 Torr of total pressure and with $T_h = 800$ °C ($t_a = 125$ μs). This spectrum is in the region of the strongest transitions of the (030)' - (000)" band of SiH_2. The base line corresponds to zero laser intensity, i.e., 100% absorption.

(0−1) band head of C−C Swan system

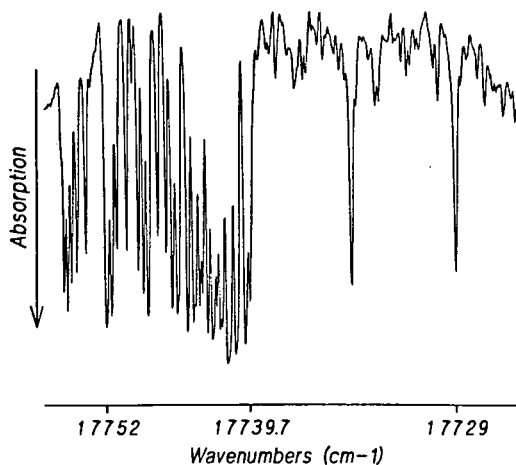
Wavenumbers (cm−1)

| 17752 | 17739.7 | 17729 |

Figure 3. ILS spectrum of a microwave discharge of ~1% acetylene in argon at 0.7 Torr total pressure. The spectrum is centered at the (0-1) bandhead of the C₂ Swan system.
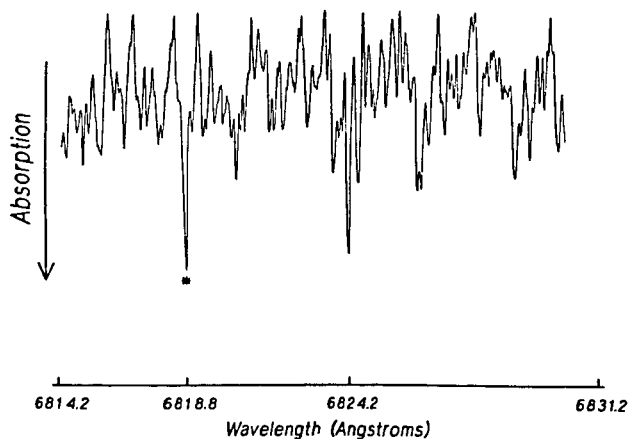
ILS spectrum of Methane at 610 torr & 295 K

Wavelength (Angstroms)

| 6814.2 | 6818.8 | 6824.2 | 6831.2 |

Figure 4. The ILS spectrum of a part of the 682 nm band of methane (assigned as $2\nu_1 + 3\nu_3$. This spectrum is a composite of individual spectral profiles and is obtained by joining together spectral profiles recorded for overlapping spectral regions. The most prominent feature is labeled by an asterisk (*).

DIAGNOSTICS AND MODELING OF PLASMA PROCESSES

Richard A. Gottscho
AT&T Bell Laboratories, Murray Hill, NJ 07974

INTRODUCTION

The full exploitation of rf and dc glow discharges for microelectronic and photonic device fabrication, coherent and incoherent light sources, and high voltage switching will only be realized when we have reliable numerical models with which processes can be simulated. It is perhaps ironic that we can simulate device operation[1] in great detail but must resort to trial and error development for device fabrication. This dichotomy is more remarkable when one realizes that the physics of semiconductor devices and plasma reactors are identical. Chemistry complicates the modeling of plasma reactors.

This talk will focus on recent fluid models of discharge physics and *in situ*, non-intrusive diagnostic experiments designed to test these models.[2-8] Specific examples related to diamond film growth and hydrogen-containing plasmas will be highlighted as appropriate. Emphasis will be placed on experimental and theoretical results for electric fields, ion densities, reactive atomic concentrations, and degrees of dissociation.

ELECTRIC FIELDS

Consider sheath electric fields. Understanding the magnitudes and shapes of sheath fields constitutes the most basic understanding of a discharge. The local sheath field depends on not only the applied field but also the space charge distribution. In one dimension, Poisson's equation is solved to obtain the local field:

$$\frac{\partial E}{\partial x} = \frac{e}{\varepsilon_0}(n_p - n_e - n_n) \tag{1}$$

where n_p, n_e, and n_n are the positive ion, electron, and negative ion densities, respectively, and E is the electric field. Electric fields can be measured non-intrusively and with high spatial and temporal resolution by exploiting molecular and/or atomic Stark effects.[6,9-12] Positive ion densities in Eq. 1 can be measured by laser-induced fluorescence spectroscopy.[13-15] Negative ions can be probed using photodetachment spectroscopy.[7,8,16] Combined, this set of measurements provides stringent tests for theory.

LOCAL FIELD AND BEAM ELECTRON MODELS

The simplest fluid theories entail the solution of Poisson's equation above coupled with equations of continuity for ion and electron densities:

$$\frac{\partial n_i}{\partial t} + \frac{\partial(n_i u_i)}{\partial x} = F - L \tag{2}$$

where i denotes p, e, or n, u is the average (fluid) velocity, F is the rate of formation, L is the rate of loss. When the local field approximation is valid, *i.e.* the collisional mean free paths are much smaller than the distances over which electric fields and densities change significantly, the source and loss terms in Eq. (2) can be expressed as functions of just E/N. Following this approach, Boeuf[2] recently calculated sheath fields and charge densities in rf discharges through He and obtained good *qualitative* agreement with measurements of sheath electric fields in both low and high frequency discharges containing BCl_3.[6]

Although the local field approximation works reasonably well for electric fields and current-voltage characteristics, it fails miserably for the calculation of ionization and excitation rates. In the sheaths, the electric field varies so rapidly in both space (and time for rf discharges) that the electron energy distribution and electron-impact collision rates are not unique functions of the local value of E/N. To deal with this problem, Graves *et al.* and Sawin *et al.* have expressed the ionization rate coefficient as a function of the average electron energy, which is determined by solving the electron energy conservation equation simultaneously with the continuity and Poisson equations.[3–5] In this fashion, excellent agreement was obtained between calculated and measured space-time dependent optical emission intensities in high frequency discharge.[5,17]

An alternative approach to using an electron energy balance equation is to use electron beam models.[18–20] Electrons created by secondary emission processes at the cathode are considered as a separate group from bulk electrons. Continuity and energy balance equations for these ballistic or beam electrons are solved along with Poisson's equation and continuity equations for bulk electrons and ions. Results from such beam models show good agreement with experiment.[20]

MULTI-DIMENSIONAL EFFECTS

Up until now, the modeling of dc and rf discharges has been mostly limited to one-dimensional systems. Although most parallel-plate reactors can be operated in quasi-one-dimensional regimes and careful experimental design can ensure one-dimensional measurements, most plasma processes do not utilize well-confined discharges. Thus, multi-dimensional effects are important. Recent work at low frequency shows that the electron-beam model is a useful framework within which the ion transport and electric field profiles of asymmetrical parallel-plate discharges can be understood.[21] For example, radial ion density profiles are non-uniform in asymmetrical discharges because the electron beam responsible for ionization has smaller cross sectional area when the small electrode is the momentary cathode than when the large electrode is the momentary cathode. Because the electron beam is created mostly by ion-impact collisions with the electrodes, the non-uniformity is reinforced on every half-cycle. These effects lead directly to non-uniform thin film etching and deposition rates. Although beam models qualitatively explain a variety of ion density and electric field measurements in these asymmetrical discharges, it remains to model these data self-consistently and quantitatively.

REACTIVE SPECIES

Another area for model improvement involves the prediction of reactive species densities.

Although there are numerous models for predicting these quantities, they generally lack self-consistency. The models have either been semi-empirical or have made assumptions about the electric field profile. The simplest chemical discharges to model are those through diatomic gases such as N_2 or H_2. Using 2 photon laser-induced fluorescence, the concentrations of reactive atoms such as N and H can be measured and compared to the results of fluid simulations.[15,22-24] Using spontaneous Raman spectroscopy, it should be possible to calibrate these measurements and also determine the degree of dissociation.[25]

SUMMARY

The use of reliable discharge models for predicting sheath electric field profiles, ion and electron currents, reactive species concentrations, and degrees of dissociation will alleviate the tortuous nature of trial-and-error process development. The optimal process parameter space can be derived more rapidly, key parameters for improved process control can be more readily identified, and data from process monitors can be more easily interpreted and exploited in a feedback control system.

REFERENCES

[1]   For example see C.M. Snowden, Rep. Prog. Phys. **48**, 223 (1985).

[2]   J.P. Boeuf, Phys. Rev. Lett. **36**, 2782 (1987).

[3]   D.B. Graves and K.F. Jensen, IEEE Trans. Plasma Sci. **14**, 78 (1986).

[4]   A.D. Richards, B.E. Thompson, and H.H. Sawin, Appl. Phys. Lett. **50**, 492 (1987).

[5]   D.B. Graves, J. Appl. Phys. **62**, 88 (1987).

[6]   R.A. Gottscho, Phys. Rev. A. **36**, 2233 (1987).

[7]   R. A. Gottscho and C. E. Gaebe, IEEE Trans. Plasma Science **14**, 92 (1986); J. Vac. Sci. Technol. A **4**, 1795 (1986).

[8]   C.E. Gaebe and R.A. Gottscho, "Laser (and other) diagnostics of rf discharges," in *Radiative Processes in Discharge Plasmas*, edited by J.M. Proud and L.H. Luessen, Plenum (1986), p. 495.

[9]   D. K. Doughty and J. E. Lawler, Appl. Phys. Lett. **45**, 611 (1984).

[10] B.N. Ganguly and A. Garscadden, Appl. Phys. Lett. **46**, 540 (1985); B.N. Ganguly and A. Garscadden, Phys. Rev. A **32**, 2544 (1985).

[11] B.N. Ganguly, J. Appl. Phys. **60**, 571 (1986).

[12] J. Derouard and N. Sadeghi, Opt. Comm.**57**, 239 (1986).

[13] R. A. Gottscho, R. H. Burton, D. L. Flamm, V. M. Donnelly, and G. P. Davis, J. Appl. Phys. **55**, 2707 (1984).

[14] V. M. Donnelly, D. L. Flamm, and G. Collins, J. Vac. Sci. Technol. **21**, 817 (1982).

[15] R. A. Gottscho and T. A. Miller, Pure and Appl. Chem. **56**, 189 (1984).

[16] J. Taillet, C. R. Acad. Sc. Paris **269**, 52 (1969); M. Bacal, G. W. Hamilton, A. M. Bruneteau, H. J. Doucet, and J. Taillet, J. de Physique **40**, C7-791 (1979); K. E. Greenberg, G. A. Hebner, and J. T. Verdeyen, Appl. Phys. Lett. **44**, 299 (1984).

[17] E. Gogolides and H.H. Sawin, American Vacuum Society National Symposium, Atlanta, GA, October 1988, abstract # PS-WeA3.

[18] A.V. Phelps, B.M. Jelenkovic, and L.C. Pitchford, Phys. Rev. A **36**, 5327 (1987).

[19] J.P. Boeuf and P. Segur, in "Interactions Plasma Froids Materiaux," ed. by C. Lejeune, Les Editions de Physique (1988), p. 113.

[20] R.A. Gottscho, A. Mitchell, G.R. Scheller, N.L. Schryer, D.B. Graves, and J.P. Boeuf, Proc. 7th Symp. Plasma Proc., Electrochem. Soc. (1988), edited by G.S. Mathad, G.C. Schwartz, and D.W. Hess, page 1.

[21] R.A. Gottscho, G.R. Scheller, D. Stoneback, and T. Intrator, J. Appl. Phys. (to be submitted).

[22] J. Bokor, R.R. Freeman, J. C. White, and R. H. Storz, Phys. Rev. A **24**, 612 (1981); W. K. Bischel, B.E. Perry, and D.R. Crosley, Chem. Phys. Lett. **82**, 85 (1981) and Appl. Opt. **21**, 1419 (1982); M. Alden, H. Edner, P. Grafstrom, and S. Svanberg, Opt. Comm. **42**, 244 (1982); P. Brewer, N. Van Veen, and R. Bersohn, Chem. Phys. Lett. **91**, 126 (1982); M. Heaven,, T.A. Miller, R.R. Freeman, J. White, and J. Bokor, Chem. Phys. Lett. **86**, 458 (1982).

[23] L. F. DiMauro, R. A. Gottscho, and T. A. Miller, J. Appl. Phys. **56**, 2007 (1984).

[24] R. Walkup, K. Saenger, and G.S. Selwyn, Mat. Res. Soc. Symp. Proc. Vol. **38**, 69 (1985).

[25] B.L. Preppernau, D.A. Dolson, R.A. Gottscho, and T.A. Miller, Plasma Chem. Plasma Proc. (in press).

[26] P.J. Hargis and K.E. Greenberg, 41st Annual Gaseous Electronics Conference, Minneapolis, MN (October 1988), Abstract # LA-3.

CARS DIAGNOSTICS IN REACTING MIXTURES

James J. Valentini

Department of Chemistry
University of California
Irvine, CA 92717

INTRODUCTION

Coherent anti-Stokes Raman scattering (CARS) is a coherent optical variant of the inelastic light scattering process known as the Raman effect. CARS spectroscopy possesses the universality of Raman spectroscopy but with greatly enhanced sensitivity. It is insensitive to background luminescence, can be configured to allow remote measurements, has excellent temporal and spatial resolution, and can provide detailed information on both the chemical composition and physical state of gas, liquid, and solid samples. Because of these desirable attributes CARS has become an important optical diagnostic method, in particular for characterizing combustion media, plasmas, and chemically reacting mixtures. This article provides a brief introduction and overview of such applications of CARS, with a particular emphasis on the last of these.

PHENOMENOLOGY

CARS is non-linear optical process, a four-wave mixing process, in which optical radiation at three incident frequencies, $\omega_1, \omega_2, \omega_3$, interacts with a sample to generate optical radiation at a fourth frequency, ω_0:

$$\omega_0 = \omega_1 - \omega_2 + \omega_3. \tag{1}$$

It is not necessary to have three distinct incident frequencies, and in fact CARS is most generally carried out with $\omega_1 = \omega_3$. It is conventional then to describe ω_1 as the "pump" or "laser" frequency, and designate it ω_L and to call ω_2 the Stokes frequency, and write it as ω_S, so that Eq. 1 becomes

$$\omega_{AS} = \omega_L - \omega_S + \omega_L = 2\omega_L - \omega_S, \tag{2}$$

with ω_0 replaced by ω_{AS}, the so-called anti-Stokes frequency. Both ω_L and ω_S are provided by high intensity laser beams, and the signal at ω_{AS} is laser-like also, in that it too is coherent. The four-wave mixing process of CARS generates a signal at ω_{AS} under all conditions for all media. However, the magnitude of the signal is greatly enhanced when the frequency difference $\omega_L - \omega_S$ is resonant with the frequency, ω_R, of a Raman-allowed transition in the sample in which the four-wave mixing is taking place,

493

$$\omega_S = \omega_L - \omega_R, \tag{3}$$

for which

$$\omega_{AS} = \omega_L + \omega_R. \tag{4}$$

Although the Raman transition may be between different electronic states of a molecule or atom, it is most commonly a transition between different vibrational or rotational states of a molecule.

An energy level schematic for CARS illustrating the relation between ω_L, ω_S, and ω_{AS} is shown in Fig. 1. The molecular rovibrational states connected by the Raman transition are labeled r and g. The states labeled o and p are the lowest excited electronic states of the molecule, and those labeled v are virtual electronic states. Since only the frequency difference $\omega_L - \omega_S$ matters, the frequencies can be chosen arbitrarily, and only one of these frequencies need be tunable. To take advantage of efficient fixed-frequency and tunable pulsed lasers these frequencies are usually chosen to be in the visible region of the spectrum. A very common choice is a Nd:YAG/dye laser system, in which the second harmonic of the Nd:YAG laser at 532 nm serves both as ω_L and as the pump source for the dye laser, which generates ω_S.

Figure 2 shows a block diagram of the essential elements of a CARS spectroscopy apparatus. Note that the ω_L and ω_S beams are crossed at some angle θ, and that the angle between the ω_L and ω_{AS} beams is ϕ. The angle θ is chosen to satisfy the phase-matching requirement,

$$\underline{k}_L + \underline{k}_L = \underline{k}_S + \underline{k}_{AS}, \tag{5}$$

where k_α is the wave-vector for the optical beam at frequency α. The magnitude of the wave-vector is given by

$$k_\alpha = \omega_\alpha \, n_\alpha / c, \tag{6}$$

with n_α the index of refraction at frequency α. For gases at pressures less than about 1 atmosphere, the medium is essentially dispersionless, that is $n_\alpha = 1$ for all α. For such dispersionless media $\theta = \phi = 0$ and all the beams are collinear.

APPLICATIONS

As a light scattering technique CARS has very high intrinsic temporal resolution, determined solely by the temporal widths of the laser pulses used to generate the signal. This makes CARS a very attractive technique for the investigation of rapidly time-varying phenomena, such as chemical reactions and photochemistry. This has been the principal application of CARS in our laboratory. The high temporal resolution is complemented by the universality of Raman scattering, making CARS suitable for monitoring chemical species not easily detected by other spectroscopic

techniques. Figure 3 shows an example of such an application. This is the vibrational Q-branch spectrum of O_2 ($^3\Sigma_g$) formed in the photolysis of ozone. The spectrum is recorded 2 nanoseconds after photolysis, and characterizes the nascent rotational and vibrational distribution of this O_2 photofragment, without any collisional relaxation. The peaks at 1550 - 1560 cm^{-1} are due to the 300K thermal distribution of O_2 impurity in the O_3 sample. Note that the photofragments are produced in high rotational and vibrational states that are not appreciably populated under 300K thermal equilibrium conditions. Figure 4 shows portions of a Q-branch CARS spectrum of H_2 formed in the H + HI reaction. The H atoms were generated by pulsed-laser photolysis of HI, and the H_2 detected only 3.5 ns later, a time delay which allowed at most one H atom collision. Very high rotational and vibrational states are observed, with internal energies as great as 17,750 cm^{-1}, equivalent to kT at 25,000 K. The spectrum indicates a population inversion between v = 1 and v = 0.

Transient species can also be detected under the non-thermal-equilibrium conditions of an electric discharge. Figure 5 shows a CARS spectrum taken in a pure oxygen microwave discharge. Q-branch and O-branch transitions of the ground and first excited vibrational states of $O_2(^3\Sigma_g)$, which is the ground electronic state, are evident. Also in the spectrum are transitions due to $O_2(^1\Delta_g)$, the first excited electronic state of molecular oxygen. Under the conditions of the discharge only a few percent of the 5-Torr sample is in the $^1\Delta_g$ state.

Figures 6 and 7 exemplify further the generality of CARS, showing detection of two important radical species, OH and CH_3. The former was produced by laser photolysis of hydrogen peroxide, the latter by laser photolysis of methyl iodide. In each case the sample pressure was a few hundred millitorr, at which a spectrum with very good signal-to-noise ratio could be obtained in a scan of a few minutes duration.
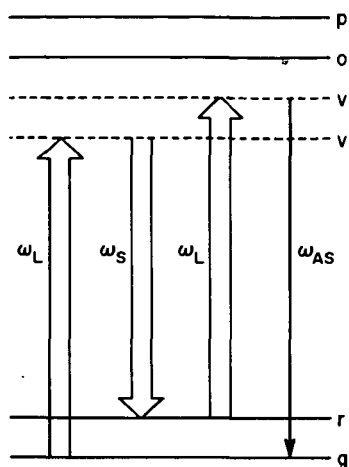
ACKNOWLEDGMENTS

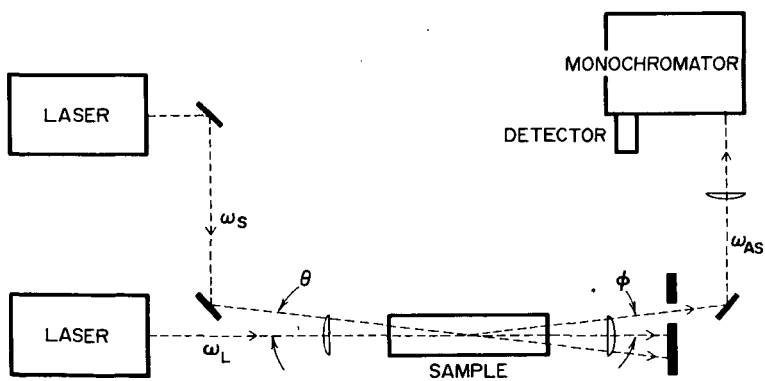Figure 1. Energy level schematic for CARS.

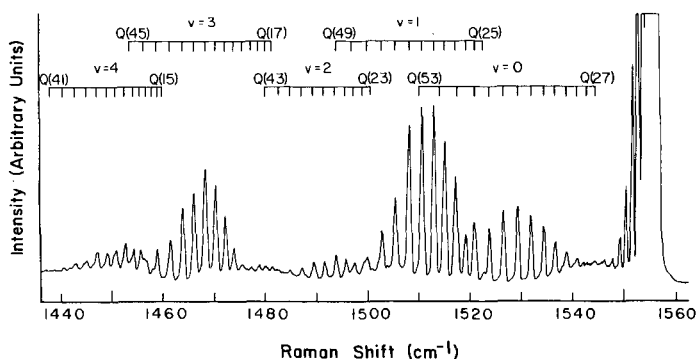Figure 2. Block diagram of a CARS apparatus.

Figure 3. Vibrational Q-branch CARS spectrum of $O_2(^3\Sigma_g)$ photofragment from the photolysis of O_3.
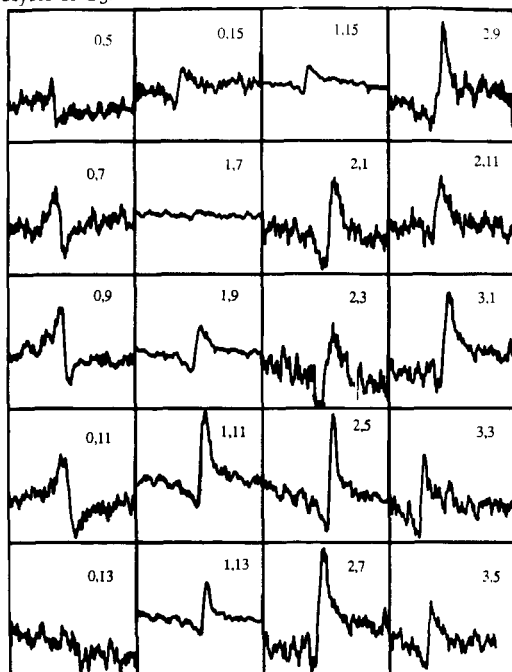

Figure 4. Vibrational Q-branch CARS spectrum of H_2 from the H + HI -> H_2 + I reaction at 1.6 eV collision energy. The peaks are labeled as v,J.

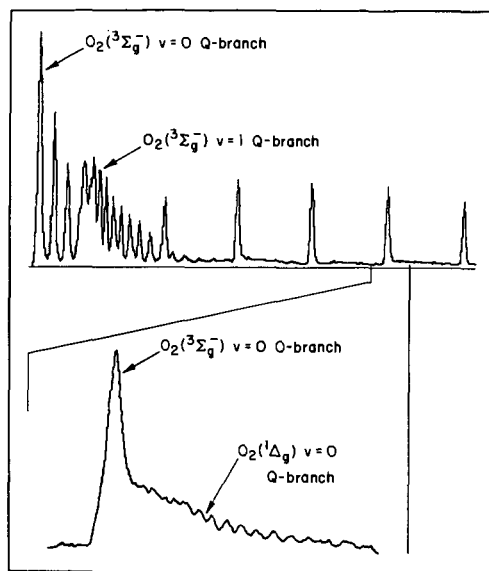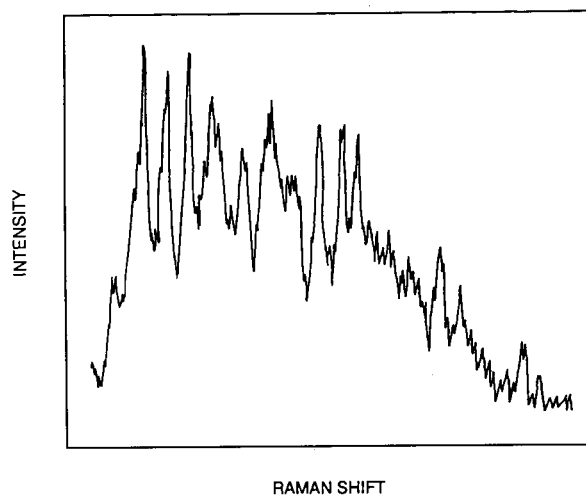Figure 5. CARS spectrum of an O$_2$ microwave discharge.

RAMAN SHIFT

Figure 6. Vibrational Q-branch CARS spectrum of the CH$_3$ ν_1 vibration at 3000 cm^{-1}. The methyl radicals were formed by photolysis of methyl iodide.
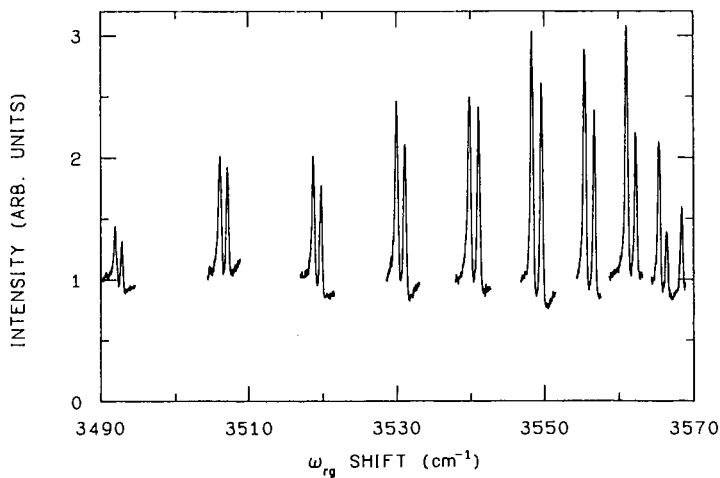

Figure 7. Vibrational Q-branch CARS spectrum of OH radicals from the photolysis of hydrogen peroxide.

LOW PRESSURE PLASMA DIAGNOSTICS BY CARS AND OTHER TECHNIQUES

Nobuhiro Hata

Materials Science Division
Electrotechnical Laboratory
1-1-4 Umezono, Tsukuba-shi, Ibaraki 305, JAPAN

ABSTRACT

Within the past several years, intensive research activities relating amorphous-silicon technology have stimulated plasma-chemical-vapor-deposition (plasma-CVD) diagnostics by laser-spectroscopic techniques. Among them, coherent anti-Stokes Raman spectroscopy (CARS) has attracted much attention because of its great success in combustion diagnostics, and has been employed for low-pressure-plasma studies. Gas-phase species such as SiH_4, H_2, Si_2H_6, SiH_2, and GeH_4 have been detected, time dependences of their concentration and spatial profiles of their concentration and rotational temperature have been determined, and the gas-phase mechanisms have been discussed. This talk will employ those results as examples, and discuss (1) the potential of CARS for gas-phase analysis in CVD (including (i) what species are monitored, (ii) what information is obtained, and (iii) what are the advantages and limitations), and (2) some other diagnostic techniques that provide additional information for better understandings of CVD mechanisms.

INTRODUCTION

Diamond synthesis from the gas phase has attracted much attention in science and applications (1-7). There are a lot of techniques to produce carbon thin films, and they are divided into chemical vapor deposition (CVD), and physical vapor deposition (PVD). In CVD methods, source gas molecules containing carbon atoms are activated thermally, optically, or by electron collision, and molecular fragments are created. They then diffuse in the gas phase to the substrate surface to feed the surface processes that grow carbon thin films. In PVD methods, particles that contain carbon atoms are fed to the surface. Sputtering and ion-beam deposition are classified in this category.

There are a lot of applications of carbon thin films. Among them, one of the most attractive ones is the micro-electronic applications. Diamond has a high resistivity, thermal conductivity, transparency, and wide band-gap width. It shows semiconducting characteristics when some impurities are doped. These features suggest that thin film diamond will possibly be used as an important material for insulator of field-effect devices, photoconductors, high-temperature devices, short-wavelength light-emitting devices, and radiation resistive devices. In order to realize those electronic applications, development of low-temperature fabrication technology with less damage to the substrate and high controllability of structure and characteristics is required very much.

Thin film carbon has a lot of structural types such as diamond, diamond-like carbon, i-carbon, amorphous carbon, and graphite. Relationships between the film structure and the fabrication methods as well as the operating conditions are partly

known empirically. Understanding of the gas-phase and surface mechanisms that govern those relationships will lead to superior fabrication technology with high controllability. And the first step to such understanding is the observation of the gas phase and surface.

Within the past several years, amorphous silicon related materials have been investigated intensively because of their potential for applications. At present, they are mostly fabricated by plasma-chemical-vapor deposition (plasma-CVD), and their properties are sensitive to the plasma operating conditions. Therefore, the research activities relating the amorphous-silicon technology have stimulated plasma-CVD diagnostics, especially those by laser spectroscopic techniques. Gas-phase process diagnostics by laser spectroscopy have several advantages and enable non-intrusive in-situ observation.

Among them, coherent anti-Stokes Raman spectroscopy (CARS) has attracted much attention because of its great success in combustion diagnostics (8), and has been employed for low-pressure-plasma studies (9). Gas-phase species such as SiH_4, H_2, Si_2H_6, SiH_2, and GeH_4 have been detected, time dependences of their concentration and spatial profiles of their concentration and rotational temperature have been determined, and the gas-phase mechanisms have been discussed (9-14).

In addition to CARS, laser induced fluorescence (LIF) was employed, and gas-phase species such as Si and Ge were measured. Optical emission spectroscopy, which is, in fact, not a laser spectroscopy, was also employed, and Si, SiH, H_2, H, and Ge in their electronically ground states were measured. It has been demonstrated that all those techniques provide information about different sets of species to one another, and therefore, more information is obtained by combining several techniques (13,14).

Low-temperature CVD processes such as plasma-CVD for amorphous-silicon-related materials are preferred for micro-electronic applications to PVD and thermal-CVD processes because of their film growth at lower temperature with less damages to the substrate. Although the crystalline size is different from that of thin film diamond, microcrystalline silicon (μc-Si) film is more like to it than amorphous silicon (a-Si) film. The deposition conditions for μc-Si is higher in excitation power and hydrogen dilution than those for a-Si. This tendency is almost the same to the deposition conditions for thin film diamond compared with those for carbon films of other structures. Another similarities are their low growth rates, which sometimes are serious problems for applications.

Once the gas-phase profiles of specie concentration and temperature were measured and understood, the efforts of the process-diagnostic research have come to be directed to some key issues in the deposition processes. They are: (1) the effects of ion bombardment to the surface (15), (2) the roles of hydrogen in the gas-phase and at the surface, (3) the dominant species that contribute to the deposition, and (4) the role of O and N atoms to the growth rate (5). Recently, methyl radical CH_3, which was long considered as the dominant specie, was experimentally detected by infrared diode laser spectroscopy (16). And atomic hydrogen was detected by laser ionization technique (17). Those are the typical examples of the recent trend in process diagnostic research.

This talk includes (1) our experimental setup for gas-phase process diagnostics, (2) a review of the important results in the diagnostics of plasma-CVD for amorphous-silicon-related materials, (3) potential of the techniques for gas-phase analysis in diamond CVD, and (4) another technique to reveal the key mechanisms.

EXPERIMENTAL

Light Sources

Gas pressure in plasma CVD is much lower than the atmospheric pressure, and therefore, high power is required for the CARS light sources. Furthermore, tunable ultraviolet light is necessary for LIF of Si and Ge, and it has to be generated by frequency mixing laser lights. Those are the requirements for a high power laser as the light source. In the experiment, Q-switched Nd:YAG laser (Quanta-Ray, Model DCR-2A) system with an amplifier and an second harmonics generator was used to produce 532 nm second harmonics with 2 ns pulse width and 350 mJ pulse energy, as well as the fundamental 1064 nm laser light. Some part of the 532 nm laser light was used to pump the pulsed dye laser (Quanta-Ray, Model PDL-1) with an amplifier and a wavelength control interface (Quanta-Ray, Model MCI-1). To obtain tunable ultraviolet light for LIF measurements, the dye laser light was frequency doubled and mixed with the fundamental 1064 nm light from the Nd:YAG laser by using the wavelength extender (Quanta-Ray, Model WEX-1). Another dye laser (Quanta-Ray, Model PDL-2) was used to obtain tunable visible light.

All those laser systems were set on a long optical bench, and mirrors and beam splitters were arranged so as to generate laser lights necessary to CARS, LIF and another technique. For CARS, 545-690 nm dye laser light and 532 nm Nd:YAG laser second harmonics were collinearly collimated using a dichroic mirror and then introduced into the plasma-CVD chamber through a focusing lens. And for LIF, 245-280 nm tunable ultraviolet light was generated and introduced into the chamber through quartz optics.

Plasma-CVD Chamber

A specially designed capacitively-coupled diode-type radio-frequency (13.56 MHz) plasma-CVD chamber equipped with three optical window ports was used. The diameters of cathode and anode were 90 and 110 mm, respectively, and their separation was 30-40 mm (variable). The chamber wall was 250 mm apart from the center, and the optical ports were 100 mm long and had quartz windows of 100 mm in diameter at the ends. The chamber was pre-evacuated to 10^{-5} Pa by a 6-inch oil-diffusion pump, and then the valve was closed, the reactant gas was introduced, and was pumped out with a root pump to keep the pressure typically at 10-100 Pa.

Detection Optics

Detection optics for CARS were designed to separate CARS signal light from laser lights, plasma emission, and ambient lights. Mixed beams of lasers and CARS signal were collimated using a lens, and laser lights were separated away using two

dichroic filters, and 1-m double monochromator (Jobin Yvon, Model U1000). Non-resonant CARS signal was rejected using an analyzer, while polarizers were placed in the light source optics to constitute the polarization CARS configuration (18). The CARS signal was detected by an intensified photo-diode array detector (Princeton Applied Research, Model 1420).

Detection optics for LIF and OES were designed to collect the emitted light from gas-phase species. Tow quartz lenses of 350 mm focal length and 60 mm diameter were used to collect the light and introduce it into the entrance slit of 32 cm grating monochromator (Jobin Yvon, Model HR320). The signal light was detected by a photomultiplier (HAMAMATSU, Model R292).

Control and Data Acquisition

The Nd:YAG laser was operated at 10 shots per second, and the CARS signal was accumulated at each dye laser wavelength for 10-100 laser shots, and then the dye laser wavelength was changed. Plasma conditions were set manually, and the measuring point was changed by moving the plasma-CVD chamber. The LIF signal from the photomultiplier was accumulated in a boxcar integrator (Princeton Applied Research, Model 4420) with the laser shots as the trigger pulses, and the noises that did not coincide with the laser shots were removed.

PLASMA-CVD FOR AMORPHOUS SILICON RELATED MATERIALS

Temperature Profile

Silane (SiH_4) molecule is abundant in the gas phase of most of the plasma-CVD for amorphous-silicon-related materials. Therefore, temperature determination from SiH_4 CARS signal was performed. A simple equation for SiH_4 CARS spectrum:

$$(\Sigma g_J exp[-hcBJ(J+1)/kT]exp\{-[\delta v - v_0 - \Delta BcJ(J+1)]^2/(\Delta v)^2\})^2 \qquad (1)$$

was assumed and the spectral shapes for different values of rotational temperature T were calculated (12). Then the measured CARS spectra were compared with those calculated curves to find the best fitted one, from which the values of rotational temperature were obtained. From the result, the effects of the substrate heating and radio-frequency discharge to the gas-phase temperature were discussed.

Hydrogen (H_2) molecule is abundant in the gas phase not only of the plasma-CVD for amorphous-silicon-related materials but also many other CVD processes. It is known in diamond CVD that heavily diluting the source gas molecule with hydrogen is very important for obtaining diamond structure. Both the ro-vibrational and pure rotational CARS spectra of H_2 show a series of peaks that corresponds to a series of the rotational quantum states (19-21). That is due to the large values of the rotational constants of H_2 molecule consisting of light H atoms. From the ratio of the CARS signal peak intensities, distribution within those rotational states, and therefore, the rotational temperature is obtained. The pure rotational CARS signal is about 100 X stronger in intensity than the ro-vibrational signal, and suited for low-pressure plasma-CVD

diagnostics. The relative peak intensities are given by the square of the non-linear electric susceptibility $\chi^{(3)}(J,J+2)$, which is written as (20),

$$\chi^{(3)}(J,J+2) \sim N(J+1)(J+2)[X(J,T)-X(J+2,T)] / Q(T)(2J+3) \qquad , \qquad (2)$$

$$X(J,T) = g_J \exp[-E(J)/kT] \qquad , \qquad (3)$$

$$Q(T) = \Sigma g_J(2J+1)\exp[-E(J,v)/kT] \qquad , \qquad (4)$$

$$E(J,v) = E_v^0 + B_v J(J+1) + D_v J^2(J+1)^2 + H_v J^3(J+1)^3 \qquad . \qquad (5)$$

By measuring the hydrogen CARS spectra from one point to another, the temperature profile in the gas phase was determined (20). From the results, it was concluded that the gas-phase temperature is mostly determined by the substrate and chamber-wall temperatures and is little affected by the other plasma operating conditions within the range used for amorphous-silicon deposition. That is consistent with the fact that the gas-phase temperature relaxation time determined by the ratio of the heat capacity to thermal conductivity is much shorter than the gas residence time in the chamber. And the gas-phase temperature in the vicinity of the film-growing surface agreed with the surface temperature measured with a thermocouple.

Concentration Profile

The concentration of molecule is determined from the CARS signal intensity by using the quadratic dependence of the CARS signal intensity I_{CARS} to the concentration [M] of the resonant molecule M:

$$I_{CARS} \sim |\chi^{(3)}|^2 \sim [M]^2 \qquad . \qquad (6)$$

By measuring the CARS signal from one point to another, the concentration profile is obtained. The absolute value of the molecular concentration is determined by using the gas of known concentration for calibration. OES signal also represents the relative concentration of the species that emit the photons when the emission efficiency is constant and the absorption of the emitted photons by other species is neglected. In addition to the necessary conditions for OES signal to be a measure of specie concentration, if the excitation light is not attenuated much along its path, the LIF signal is a measure of the specie concentration.

The concentration profiles of SiH_4, Si, and Si$^{\bullet}$ were measured between the cathode and anode along the central axis, and much different profiles were obtained among those species. Si concentration had a two distinct peaks at about 10 mm from the cathode and anode, while SiH_4 concentration changed more gradually and was almost constant in the discharge volume except the sheath regions (14). The result was interpreted that a lot of Si atoms are created by electron collision in the regions where electron energy is high. The highly energetic electrons are created by the acceleration of secondary emitted electrons from the electrodes by the sheath electric fields. SiH_4

molecule, on the other hand, is dissociated or excited even by electrons with lower kinetic energy, thus more gradual change in the discharge region is realized.

The concentration profiles of SiH_4 and GeH_4 in a plane parallel to the electrode surface were also measured, and gradual concentration changes of the both molecules toward the radial direction were observed (13). The result was interpreted in terms of dissociation and excitation of the source gas molecules supplied from outside of the discharge by molecular diffusion.

Transient Behavior

Concentrations of SiH_4 and Si_2H_6 were measured as functions of time after the discharges were switched on in a closed discharge chamber (11). The concentrations of source gas molecules decreased exponentially with time, and the decay time constants were obtained from the slope of the concentration plotted semi-logarithmically against time. From the time constants, the average loss rates were calculated and their dependences on the gas pressure and discharge power were studied. In Si_2H_6 discharges, SiH_4 molecule was observed, and the time dependence of its concentration was studied. The result was interpreted in terms of the average creation rate, and compared with the average loss rate to discuss the formation mechanism of SiH_4 in Si_2H_6 discharges.

Effect of Hydrogen Dilution

Effect of Hydrogen dilution on the OES and LIF signals of Si^*, Ge^*, Si, and Ge was studied (13). Emission signal from Ge^* from GeH_4 discharge decreased very much with dilution of the source gas GeH_4 with H_2, while emission signal from Si^* did not change very much with H_2 dilution. Si and Ge atoms in their electronically ground states measured by LIF changed like their emissive species with H_2 dilution. The results were interpreted in terms of the gas-phase mechanisms with H_2 dilution.

DIAMOND CVD

As the first step for process diagnostics, measurements of temperature and specie concentration profiles will provide much information. The laser spectroscopic process-diagnostic techniques demonstrated in plasma CVD for amorphous-silicon-related materials are applicable to other CVD systems if some suitable optical windows are equipped. The arguments are what species are detected, what the detection limit is, and what information is obtained. The situation seems better for CARS measurements in diamond CVD processes, since the gas pressure is usually higher than that in plasma-CVD for amorphous-silicon-related materials. Hydrogen (H_2), methane (CH_4), and some other carbon-containing molecules will be detected by CARS, and their concentration profiles will be measured. Temperature measurement by pure-rotational CARS signal of H_2 will also be practical, and temperature profile will be obtained. As in the case of plasma CVD for amorphous-silicon-related materials, species detected by LIF will be limited to some molecular fragments, but LIF will still add information to

CARS data. Thus the first step of the diamond-CVD diagnostics will be fulfilled with the techniques used in the plasma-CVD diagnostics.

ANOTHER TECHNIQUE

What should be carried out at the next stage is to focus on the key issues: (1) the role of hydrogen, (2) the dominant species contributing to the film growth, (3) the effects of ion bombardment, and (4) the effects of O and N. For that purpose the detection of hydrogen atom by resonance-enhanced multiphoton laser-induced-fluorescence experiment was planned and is now in progress. That method is similar to the resonance-enhanced multiphoton ionization technique (17) but promises the detection of H even in the plasma CVD environment.

SUMMARY

Laser-spectroscopic gas-phase process diagnostic techniques such as CARS and LIF have been demonstrated in the plasma CVD for amorphous-silicon-related materials. Gas-phase profiles of specie concentration as well as temperature were measured in-situ non-intrusively, and the results were interpreted in terms of gas-phase kinetics. Those techniques will be applicable to other CVD processes, especially those for diamond thin films.

Process diagnostics have come to the stage where the direct observations of the key issues in the processes are strongly emphasized. Understanding of the key mechanisms that determine the growth rate, structure, and properties of thin films is very important. The processes occurring at the film growing surface were mentioned little in this talk, but it plays the other important part in the mechanisms, and should be studied extensively.

ACKNOWLEDGEMENTS

REFERENCES

(1)   Angus, W.G., Will, H.A., and Stanko ,W.S.: J. Appl. Phys., 39 (1968) 2915.

(2)   Spitsyn, B.V., Boulov, L.L., and Derjaguin, B.V.: J. Cryst. Growth, 52 (1968) 219.

(3)   Matsumoto, S., Sato, Y., Kamp, M., and Setaka, N.: Jpn. J. Appl. Phys., 21 (1982) L183.

(4)   Sawabe, A. and Inuzuka, T.: Appl. Phys. Lett., 46 (1985) 146.

(5)   Hirose, Y. and Terasawa, Y.: Jpn. J. Appl. Phys., 25 (1986) L519.

(6)   Suzuki, K., Sawabe, Y., Yasuda, H., and Inuzuka, T.: Appl. Phys. Lett., 50 (1987) 728.

(7)   Matsumoto, S., Hono, M., and Kobayashi, T.: Appl. Phys. Lett., 51 (1987) 737.

(8)   Eckbreth, A.C.: J. Propulsion and Power, 3 (1987) 210, and references therein.

(9)   Hata, N., Matsuda, A., Tanaka, K., Kajiyama, K., Moro, N., and Sajiki, K.: Jpn. J. Appl. Phys., 22 (1983) L1.

(10)   Hata, N., Matsuda, A., and Tanaka, K.: J. Non-Cryst. Solids, 59-60 (1983) 667.

(11)   Hata, N., Matsuda, A., and Tanaka, K.: Jpn. J. Appl. Phys., 25 (1986) 108.

(12)   Hata, N., Matsuda, A., and Tanaka, K.: J. Appl. Phys., 59 (1986) 1872.

(13)   Hata, N., Matsuda, A., and Tanaka, K.: J. Appl. Phys., 61 (1987) 3055.

(14)   Hata, N. and Tanaka, K.: J. Non-Cryst. Solids, 77-78 (1985) 777.

(15)   Angus, J.C., Doidl, P., and Domitz, S.: in "Plasma Deposited Thin Films" ed. by Mort, J. and Jansen, F. (CRC Press, Florida, 1986) pp. 89-127.

(16)   Celii, F.G., Pehrsson, P.E., Wang, H.-t., and Butler, J.E.: Appl. Phys. Lett., 52 (1988) 2043.

(17)   Celii, F.G., Pehrsson, F., Wang, T.-t., Nelson, H.H., and Butler, J.E.: in "Extended Abstract of the International Symposium on the Characterization of Diamond" (Tsukuba, Japan, Oct. 27-28, 1988).

(18)   Brakel, R. and Schneider, F.W.: in "Advances in Non-Linear Spectroscopy" ed. by Clark, R.J.H. and Hester, R.E. (John Wiley & Sons, Chichester, 1988) pp. 149-192.

(19)   Pealat, M., Taran, J.P.E., Taillet, J., Bacal, M., and Bruneteau, J. Appl. Phys., 52 (1981) 2687.

(20)   Marowsky, G., Gierulski, A., Dick, B., Sowada, U., and Vehrenkamp, R.: Appl. Phys., B39 (1986) 47.

(21)   Hata, N., Matsuda, A., and Tanaka, K.: in "Symposium Proceedings, 8th International Symposium on Plasma Chemistry" ed. by Akashi, K. and Kinbara, A., (IUPAC, Tokyo, 1987) pp. 500-505.

CARS DETECTION OF GASEOUS SPECIES FOR
DIAMOND DEPOSITION PROCESS

Ward C. Roman and Alan C. Eckbreth

United Technologies Research Center
Propulsion Science Laboratory
East Hartford, CT 06108

ABSTRACT

In order to understand the complicated chemical and physical processes that occur during the deposition of hard face coatings such as diamond, diagnostics that are remote, nonintrusive and sensitive to potential chemical species are necessary. One particularly promising approach is coherent anti-Stokes Raman spectroscopy (CARS) useful for measurements of temperature and species concentrations. Results to be described will include CARS measurements on a PACVD reactor used for depositing high quality diamond films. A mixture of acetylene (C_2H_2) and Argon, tested over a range of total pressures down to 0.1 Torr, was used to calibrate the CARS system. With the existing CARS system, detectivity of C_2H_2 to 5 mtorr was demonstrated. This paper describes details of the scanned narrowband colinear CARS system and examples of CARS spectra obtained for CH_4 and C_2H_2 species under rf PACVD diamond deposition conditions and also using an alternate filament–assisted technique.

INTRODUCTION

Nonequilibrium reactive plasmas are recognized as a novel approach for a wide variety of material coating applications (1). This type of plasma provides a unique environment wherein deposition of thin, hard face, conformal coatings can occur at much lower temperatures (critical for inhibiting stresses) and within more complex chemical environments than are possible by conventional vapor deposition techniques. A need exists for in-situ nonintrusive techniques for diagnosing and controlling PACVD systems used for thin coating deposition (2). If improvements can be made in durable hard face coatings, increased utilization of lightweight materials under advanced development may follow. A complete understanding of the process requires information on a large number of physical and chemical processes involving gas phase and gas–surface interactions and the associated synergistic effects. Knowledge of plasma species concentrations and "temperature" is required for correlation with the corresponding physical and chemical properties of the coatings.

Emission spectroscopy is often used for the measurement of atomic and molecular species, but the emission from excited atomic levels is often much larger than for excited molecular levels, thus the atomic species dominate the spectra and molecular signatures are difficult to extract. Species concentration is difficult to infer from plasma emission spectra because they involve excited electronic levels that are not generally in thermodynamic equilibrium with the ground state. An alternative diagnostic technique, sensitive to the molecular ground state, is Coherent Anti-Stokes Raman Spectroscopy (CARS), a nonlinear optical technique useful for measuring the concentration and "temperature" of molecular constituents since all molecules have at least one Raman active vibrational mode.

The outstanding combination of unique material properties of diamond offers the potential for applying diamond coatings in many commercial applications ranging from protective and tribological coatings to films/ heat sinks for semiconductors to optical lenses to electronic devices for space environments. Before diamond coatings can be applied to commercial type applications, many questions need to be answered.

Ti–6A1–4V was selected as the reference substrate material. It represents a critical alloy of paramount interest in many commercial/aerospace applications. Its strength to weight and low temperature oxidation/ corrosion resistance are excellent. However, erosion and wear occur rapidly, thus the need for durable hard face coatings.

APPARATUS

Figure 1 is a schematic of the nonequilibrium PACVD reactor under current investigation at UTRC. The longitudinal, tube type radio frequency (rf) geometry was selected as a design viable for later scale up to continuous production operation. In addition it permits high reactant gas flows and plasma power levels; increasing these parameters nominally results in enhanced deposition rates. The 3.6-cm-ID test section is constructed of high purity fused silica and high vacuum flanges for rapid disassembly. Up to 5 different reactant gases can be simultaneously injected at the inlet region. A 5 kW rf power supply operating at 13.56 MHz is used to inductively couple the rf power into the plasma through a multiple-turn water-cooled copper work coil. Exploratory test results revealed the importance of minimizing contamination in the PACVD system as required for providing high quality coatings onto the 1.3-cm-dia x 2-mm-thick Ti-6A1-4V substrates. As a result, a completely oil-free, venturi, vacsorb, cryopump and vacion pump system are used, including a MKS flow metering system with special traps (e.g., GaInAl) and getters to remove water vapor and oxygen. To augment pumpdown time and provide operating range flexibility, a 380 ℓ/s turbomolecular pumping system, modified for corrosion resistant operation, is used; a residual gas analyzer to monitor trace impurities is also used. This system is capable of initial operating pressures down to 10^{-7} torr. The cleanliness of the substrate prior to coating deposition is believed to be a key requirement for achieving good coating adherence to the substrate. Therefore, a test sample holder and isolated load-lock and transport system are interfaced with the PACVD system (3). This technique allows direct Secondary Ion Mass Spectrometry/Ion Scattering Spectrometry (SIMS/ISS) analysis of the substrates immediately following in-situ plasma cleaning and provides a unique capability not reported in the literature. Additional advantages of this type system include the provision for conformal coverage for complex shapes, graded composition control, and provision for independent biasing and temperature monitoring of the substrate.

As hardness and adhesion are critical parameters for characterizing thin, hard face coatings, a state-of-the-art ultramicrohardness tester and UTRC custom built adhesion test apparatus have been installed and preliminary calibration testing initiated. The ultramicrohardness tester (Nanoindenter) can resolve forces as small as $2.5\mu N$ and displacements of 0.4 nm. The adherences measurements are made on a computer-controlled pin-on-disc apparatus that has a 3-axis force transducer and a device to measure the advance of the pin into the coating. A modification to this device using an ultrasonic sensor allows for coating delamination detection. Reference 3 describes details of this equipment and initial test results.

DIAGNOSTICS

The theory of CARS is explained in several recent reviews (4,5). Figure 2 is a simplified schematic of the colinear phase-matched CARS system used in these experiments. As illustrated in Figure 2, incident laser beams at frequencies ω_1 and ω_2, termed the pump and Stokes respectively, where $\omega_1 > \omega_2$, interact through the third-order, nonlinear susceptibility of the medium to generate the coherent CARS radiation at frequency $\omega_3 = 2\omega_1 - \omega_2$. The frequency difference $\omega_1 - \omega_2$ is adjusted to access the Raman-active vibrational-rotational resonances in a given constituent. Since the characteristic vibrational frequencies of most molecules are well separated, individual species are easily addressed. The CARS process must be phase matched so that the developing signal grows constructively. The scanned, narrowband CARS approach, rather than a broadband approach, was selected due to its very high spectral resolution and maximum species detectivity. It is best used to study temporally-steady processes such as PACVD, but it has the disadvantage of being quite time consuming. Species measurements can be made from the absolute signal strength. In addition to the resonant signal from the Raman modes of interest, there is also a nonresonant electronic background contribution from all the molecules or atoms present in the control volume. This leads, due to destructive interference effects in the coherent wave mixing, to spectral signatures which are also concentration sensitive. Thus fractional concentrations can be obtained from spectral shapes without regard to signal level fluctuations caused by beam steering or particle attenuation.

As shown in Figure 2, the dye laser is scanned to generate the CARS spectrum. In this way all of the available laser pump energy excites a single transition of the resonant molecule and increases the sensitivity

by several orders of magnitude. For equivalent laser powers, decreasing the Stokes bandwidth from the typical broadband value of 150 cm^{-1} increases the CARS signal by over 10^3 due to the increased spectral intensity. Spectral scanning from 60–100 cm^{-1} requires about 30 minutes.

The basic equipment includes an injection–seeded, single–mode, Nd:YAG primary beam pump laser which is frequency doubled to produce narrow bandwidth ($\sim$ 50 MHz), 10^{-8} sec pulses at 532 nm at a 10 Hz repetition rate and a narrow bandwidth (0.4 cm^{-1}) scanned Stokes dye laser. A major portion of the primary beam is split off to drive the dye laser. The remaining 532 nm beam serves as the pump and is combined colinearly with the Stokes beam at a dichroic prior to focussing in the plasma test region. The frequency–shifted CARS signal is formed in the laser focus and all three beams exit the reactor where a dichroic separates the CARS from the incident wave mixing beams. Digital acquisition of the CARS and reference signals are obtained from fast, gated PMT detectors. The digital acquisition system also records the wavelength shift of the scanned dye laser for calibration of the CARS spectrum. All signals from the PMT are digitized on every pulse and processed in a computer. As the dye laser is scanned, successive transitions of the molecular resonances are excited and modulate the intensity of the CARS signal. The result is a spectrum of the ro-vibrational manifold of the medium from which identification of species, their concentration and temperature (vibrational and rotational) can be obtained. Typically, ten CARS pulses are averaged per spectral step which corresponds to 0.1 cm^{-1}. With appropriate referencing, the molecular concentration can be measured to within $\pm 1\%$ of the total gas density and the population in the vibrational and rotational states determined for assignment of temperatures.

RESULTS TO DATE AND DISCUSSION

In the exploratory experiments directed at diamond coatings, a mixture of 1% CH$_4$ in H$_2$ was used at a total pressure of 5 torr. The rf coils were located at the optical port location. Figure 3 is an example of the CARS methane signal obtained for the ν_1 mode. It illustrates the effect of increasing rf power from zero up to 400 Watts on depleting the methane concentration. Measurements were also made of the weaker 2 ν_2 and ν_3 modes as shown in Figure 4.

Very little is known about the chemical mechanisms of diamond film growth. Several global kinetic theories have been proposed based on nucleation theory and equilibrium. Other proposed mechanisms rely on the presence of C$_2$H$_2$ or CH$_3^+$. Spear and Frenklach at Pennsylvania State University (6) have proposed an alternative mechanism for diamond growth. It basically consist of two alternating steps. First, the surface is activated by H–atom removal of a surface–bonded hydrogen. The surface activated carbon radical then acts as a site for adding more carbons to the structure by reacting with acetylene (C$_2$H$_2$) in the plasma. To provide more quantitative experimental information to verify these proposed theories and improve the basic understanding of the diamond growth process, a series of CARS experiments was conducted focused on measurement of the C$_2$H$_2$ molecular species. C$_2$H$_2$ is a linear molecule with five fundamental vibrations. Three of the five modes are Raman active. Figure 5 displays a scan generated CARS spectrum of 5% C$_2$H$_2$ in an Ar background (ν_1 band) measured using the CARS system shown in Figure 2. This measurement was made at room temperature and 10 torr reactor total pressure while flowing the mixture of 5% C$_2$H$_2$ in Argon. High purity C$_2$H$_2$, as checked via a gas chromatograph, in concentrations of both 5% and 0.5% in Argon were used in these measurements. The measurements obtained using both concentrations indicate a C$_2$H$_2$ detectability of 5 mtorr was achieved with the present system. Continued improvements in spectral filtering should significantly improve its sensitivity level.

To determine the effect of rf plasma location on the ability to detect the C$_2$H$_2$, a series of tests was conducted for the different configurations shown in Figure 6. In each case the total pressure was 3 torr. The 5% C$_2$H$_2$ in Argon was only detected when the rf plasma was located downstream of the laser optical ports. In the other locations, the concentration of C$_2$H$_2$ was less than 5 mtorr. The next step was to investigate the configuration and test parameters under which high quality diamond coatings have been deposited. The results for the CARS spectrum of C$_2$H$_2$, ν_1 mode observed at 3 torr, is shown in Figure 7. The rf power input

to the plasma was 300 watts and the H_2 and CH_4 flow rates were 99 and 1 sccm respectively. The rf coils were located at the optical port axis and the Ti–6A1–4V substrate was located within the plasma plume and 1–cm downstream of the optical centerline. Additional experiments have also included measurements with the substrate located approximately 1 mm from the laser beam. No significant C_2H_2 CARS signal was observed in any of these tests. This would indicate, if C_2H_2 were present, that it was at concentration levels less than the 5 mtorr current detection limit of the CARS system.

To apply this CARS technique to other diamond deposition systems, a hot filament reactor configuration, similar to that reported by Celii, et al. (7) was fabricated and measurements were made of the C_2H_2 CARS spectrum. Figure 8 is a schematic of the test geometry. The gas flow was 1% CH_4 in H_2 at a pressure of 150 Torr and maintained at 200 sccm. A 2–mm–dia. x 2–cm–long tungsten filament heated to approximately 2630K was located 2 cm from the Ti–6A1–4V substrate. Figure 9 shows the scan generated CARS spectrum of the C_2H_2 v_1 band, thus verifying the presence of C_2H_2 close to the surface of the substrate as reported by Celii, et al.

Figure 10 is an example of the test results obtained using Raman scattering on a Ti–6A1–4V substrate that was coated with the polycrystalline diamond film using the rf PACVD process. In these measurements, a tunable cw dye laser operated in a single frequency configuration with a line width of < 5 MHz, tuned to 16956.18 cm^{-1}, was used as the excitation source. Raman spectra reported by Matsumoto (8) for thin diamond films indicate only one sharp peak at about 1333 cm^{-1}. This is very close to the value 1332.5 cm^{-1} reported for natural diamond by Solin and Ramdas (9). A feature of the UTRC diamond coating obtained via rf PACVD is that no graphite peak was detected in any of the Raman measurements. X–ray diffraction measurements indicated the observed interplanar spacings are in close agreement with reported values (2.065 and 1.262 Å) of natural diamond (ASTM 6–675) and UTRC reference natural diamond material.

Based on the above experiments, the following are the preliminary results: 1) a CH_4 CARS spectrum was observed in the rf plasma, 2) increasing the rf plasma power reduced the CH_4 CARS signal, 3) the rf plasma significantly reduces the C_2H_2 CARS signal in C_2H_2/Ar flow, 4) the C_2H_2 CARS spectrum was not observed in rf plasma CH_4/H_4 diamond deposition tests to date. The present C_2H_2 detectability limit is 5mtorr, and 5) the C_2H_2 CARS spectrum was observed in the hot filament reactor configuration.

SUMMARY

Laser/optical diagnostic techniques, such as the CARS system described in this paper, are candidates for application as plasma gas phase materials processing diagnostic tools, each with its own inherent advantages and associated limitations. Recognizing that no one diagnostic technique will suffice, it will only be through the complementary use of several of these techniques that a fundamental understanding of the relationship between plasma process variables and properties of the processed material coating will evolve. This may ultimately lead to simple process control strategies, including in–situ laser diagnostics and sensors, to ensure high quality, economic, reproducible plasma deposition of advanced coatings such as diamond in a production scale environment. Research addressing these aspects is continuing.

REFERENCES

(1) National Research Council, National Materials Advisory Board Report NMAB–415, *Plasma Processing of Materials*, National Academy Press, March 1985.

(2) Roman, W., *Laser/Optical Diagnostic Techniques for Plasma Materials Processing*. Invited Paper at Spring 1987 Materials Research Society Meeting, Anaheim, CA, Published in Proceedings of Symposium K – *Plasma Processing and Synthesis of Materials*, April 20–24, 1987.

(3) Roman, W., Stufflebeam, J., and Eckbreth, A., *Diagnostic Techniques for PACVD Systems for Depositing Protective Coatings*, Paper C2.2 – Proceedings of Materials Research Society Spring Meeting, Vol. 117, Process Diagnostics: Materials, Combustion, Fusion. Reno, NV, April 1988.

(4) Eckbreth, A. and Stufflebeam, J., *CARS Diagnostics for Combustion and Plasma Processes*, Paper C4.2, Proceedings of Materials Research Society Spring Meeting, Vol. 117, Process Diagnostics: Materials, Combustion, Fusion. Reno, NV, April 5–9, 1988.

(5) Eckbreth, A. and Roman, W., *Laser Diagnostics for Plasma Processing of Materials*, Keynote Invited Paper, Proceedings of ASM National Thermal Spray Conference, Cincinnati, Ohio, October 23–27, 1988.

(6) Spear, K., and Frenklach, M., *Mechanistic Hypotheses on Diamond Growth from the Vapor*. Presented at 3rd SDIO/IST – ONR Diamond Technology Initiative Symposium, Arlington, VA. July 1988.

(7) Celii, F. G., Pehrsson, P. E., Wang, H. T. and Butler, J. E., *Infrared Detection of Gaseous Species During the Filament – Assisted Growth of Diamond*, Appl. Phys. Lett., Vol. 52, No. 24, June 13, 1988.

(8) Matsumoto, S., Y., Kamo, M., Tenaka, J., and Setaka, N., *Chemical Vapor Deposition of Diamond from Methone–Hydrogen Gas*, Proc. 7th International Conference on Vac. Metallurgy, pp. 386–391, Tokyo, Japan, 1982.

(9) Solin, S., and Ramdas, A., *Raman Spectrum of Diamond*, Phys. Rev. B1, pp. 1687–1698, 1970.

(6) Spear, K., and Frenklach, M., *Mechanistic Hypotheses on Diamond Growth from the Vapor*. Presented at 3rd SDIO/IST – ONR Diamond Technology Initiative Symposium, Arlington, VA. July 1988.

(7) Celii, F. G., Pehrsson, P. E., Wang, H. T. and J. E. Butler, *Infrared Detection of Gaseous Species During the Filament – Assisted Growth of Diamond*, Appl. Phys. Lett., Vol. 52, No. 24, June 13, 1988.

(8) Matsumoto, S., Y., Kamo, M., Tenaka, J., and Setaka, N., *Chemical Vapor Deposition of Diamond from Methone–Hydrogen Gas*, Proc. 7th International Conference on Vac. Metallurgy, pp. 386–391, Tokyo, Japan, 1982.

(9) Solin, S., and Ramdas, A., *Raman Spectrum of Diamond*, Phys. Rev. B1, pp. 1687–1698, 1970.
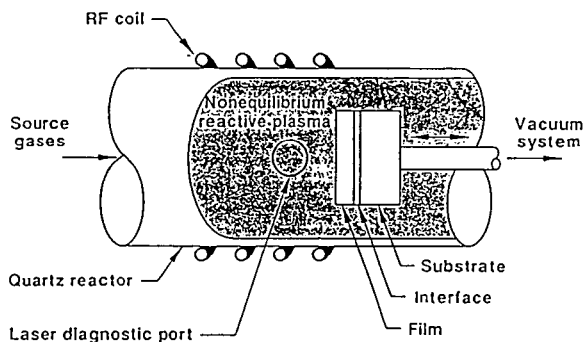
FIGURE 1. SCHEMATIC OF PACVD REACTOR USED
FOR DIAMOND DEPOSITION EXPERIMENTS .
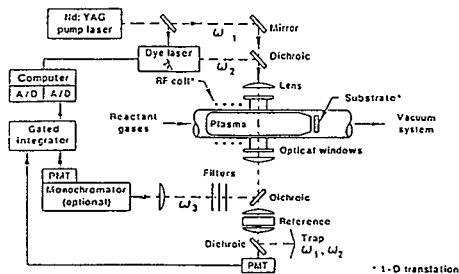
FIGURE 2. SCHEMATIC OF NARROWBAND, COLINEAR
SCANNED CARS SYSTEM USED IN PACVD
DIAMOND FILM DEPOSITION
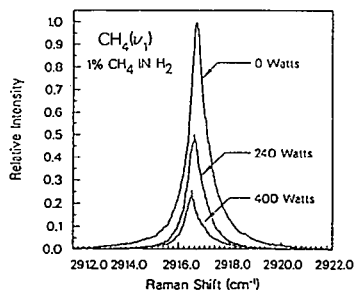
FIGURE 3. EFFECT OF RF PLASMA POWER
ON CARS METHANE SPECTRUM
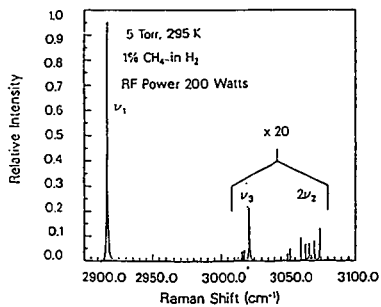
FIGURE 4. CARS METHANE SPECTRUM
OF DIFFERENT MODES
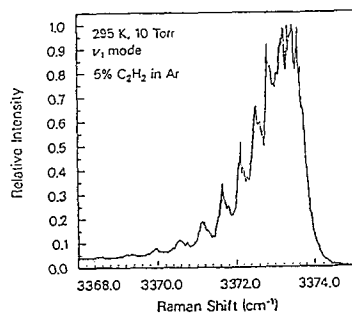
FIGURE 5. CARS SPECTRUM OF ACETYLENE
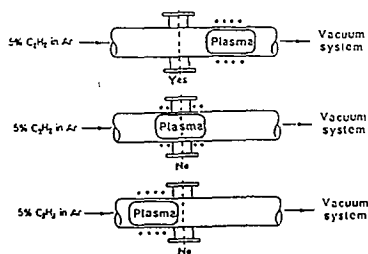
FIGURE 6. C_2H_2 DETECTION LOCATIONS
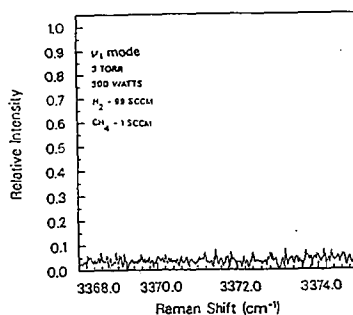
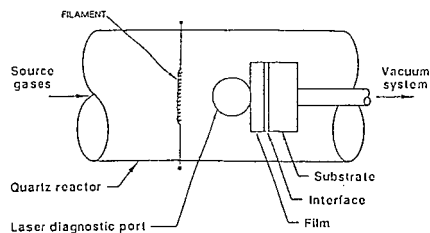FIGURE 7. CARS SPECTRUM OF ACETYLENE IN PACVD
DIAMOND COATING DEPOSITION

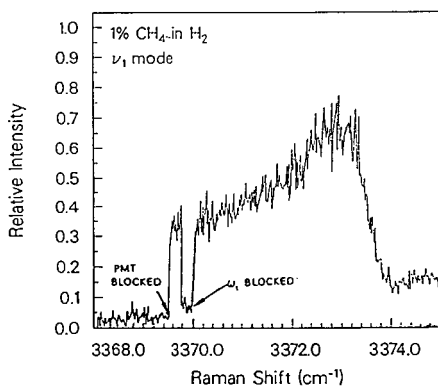FIGURE 8. SCHEMATIC OF HOT FILAMENT
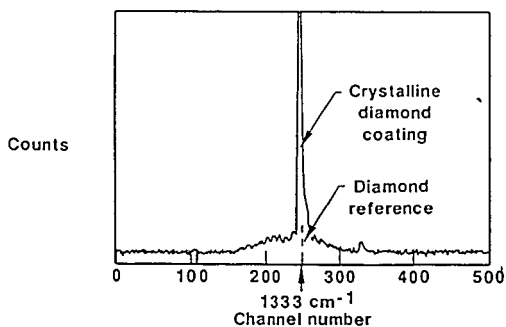REACTOR CONFIGURATION

FIGURE 9. CARS SPECTRUM OF ACETYLENE
IN HOT FILAMENT CONFIGURATION

FIGURE 10. RAMAN SPECTRA OF DIAMOND COATING
DEPOSITED VIA PACVD ON Ti-6Al-4V SUBSTRATE.

IN SITU CHARACTERIZATION OF DIAMOND NUCLEATION AND GROWTH BY XPS

David N. Belton, Stephen J. Harris,
Steven J. Schmieg, and Anita M. Weiner
Department of Physical Chemistry
General Motors Research Laboratories
Warren, MI 48090

Abstract

Filament assisted chemical vapor deposition (CVD) diamond film growth on Si(100) was studied using X-ray Photoelectron Spectroscopy (XPS) to examine the sample at selected intervals during the nucleation and growth processes. The sample was transferred under vacuum from the growth chamber to the attached XPS analysis chamber without exposure to air. Before growth XPS showed that the Si sample is covered by a layer of SiO_2 and carbonaceous residue; however, after 15 minutes of growth both of these substances are removed and replaced by a distinct SiC layer [Si(2p)=100.3 eV and C(1s)=282.7 eV]. Between 15 minutes and 4.5 hours the SiC layer grows and diamond nucleation begins. The XPS signal from diamond [C(1s)=284.3 eV] saturated after 17 hours. The identification of diamond was confirmed with Raman spectroscopy. This work identifies SiC as the substrate for diamond nucleation and growth during filament assisted CVD diamond growth on Si.

Introduction

Diamond films grow at relatively low pressures (≤ 1 atm) and temperatures (≤ 1300 K) when the proper mixture of CH_4 and H_2 flows over a substrate that is near a hot filament [1-3] or electric discharge [4-6]. This method of diamond production offers the possibility for inexpensive diamond coatings on tools, wear surfaces, and optical components. Single crystal diamonds ultimately could be prepared for use as high performance electronic devices. New technologies involving chemical vapor deposition (CVD) diamond films have not yet been implemented in part because there is no understanding of the chemical and physical processes which control the properties of the diamond films. In particular, there have been no adequate characterizations of the surfaces on which the films grow.

In order to examine the surface chemistry of diamond film growth we coupled a diamond growth chamber to an ultrahigh vacuum (UHV) system equipped with X-ray photoelectron spectroscopy (XPS). By stopping the growth at selected intervals we are able to obtain a time dependent characterization of the surface during the nucleation and growth processes without exposure to air. This experiment, which is the first to offer such a time dependent monitoring of the surface during diamond growth, allows us to characterize the surface on which diamonds are actually grown as opposed to the substrate we place in the growth chamber. These data may assist in developing better models for diamond growth [7]. In this experiment we examined growth on Si because such a large amount of work has been done on this material. We identified three distinct phases of diamond film growth: removal of initial substrate contaminants, formation of a SiC layer, and nucleation and growth of diamonds. From these results we can conclude that diamonds form on SiC as opposed to clean Si, Si oxides, or a carbonaceous layer.

Experimental Aspects

The experiments were performed in a system that coupled a UHV analytical chamber to a diamond growth chamber. The UHV chamber is a custom built system that contains a Leybold-Heraeus EA11, 150 mm hemispherical analyzer with multichannel detection and is isolated from the growth chamber with a gate valve. The sample was transferred between the two chambers on a bellows motion. The growth chamber is a 6-way 2 3/4 inch cross pumped with a 50 l/sec turbo pump. The gas supply was a premixed 0.2% CH_4 in H_2 cylinder that was connected to the growth chamber with a 100 sccm flow controller. The outlet of the growth chamber was connected through a stainless steel leak valve to a rotary vane pump that controlled the total pressure at 50 Torr as measured by a capacitance manometer. A 0.020 inch diameter W filament was mounted 2 mm from the Si(100) substrate at a temperature of 2350 K as measured by an optical pyrometer. The Si sample was cut from a Si(100) wafer, polished using 1 micron diamond paste, and washed with acetone followed by methanol prior to mounting on the transfer device. After growing for a prescribed time the pressure was reduced to 10^{-7} Torr before opening the gate valve and introducing the sample into the analytical chamber. XPS data were obtained about 30 minutes after stopping the growth.

Results and Discussion

Prior to growth (t=0) the Si(100) substrate was introduced into the analytical chamber and characterized with XPS by obtaining a survey scan and high resolution scans of the C(1s), Si(2p), and O(1s) regions. The survey scan shows that only C, O, and Si are present on the surface. The C(1s) region (fig. 1a) contains one relatively broad transition at 285.1 eV due to adventitious carbon whose probable source is hydrocarbons deposited on the sample prior to introduction. The Si(2p) region (fig. 2a) indicates the presence of both reduced Si (at 99.0 eV - used for calibration) and SiO_2 (at 102.7 eV) [8]. Similar data were obtained from three different Si samples suggesting that a carbon covered SiO_2 surface is typical for Si substrates treated in the manner reported above.

Following the initial Si(100) characterization the sample was returned to the growth chamber for a 15 minute growth. XPS data obtained at that point (fig. 2b) show no Si(2p) peak from SiO_2 (102.7 eV), but instead a new peak at 100.3 eV which we assign to SiC [8]. The elemental Si peak at 99.0 eV is reduced by 50% (fig. 2b) compared to the sample prior to growth (fig. 2a) indicating that the SiC is on top of the Si. Identification of the Si(2p) peak at 100.3 eV as SiC, is confirmed by the observation of a new C(1s) peak at 282.7 eV (fig. 1b) of the proper intensity and energy for carbide-type carbon [8,9]. In addition, the adventitious carbon seen in fig. 1a is removed during the first 15 minutes of growth. These four spectra (figs. 1a,b and 2a,b) show that after only 15 minutes of diamond growth the SiO_2 and carbon contamination are replaced by a SiC layer.

After 45 minutes XPS (figs. 1c and 2c) shows an increased SiC intensity in both the Si(2p) and C(1s) regions. Between 45 minutes and 4.5 hours the SiC Si(2p) peak increases in intensity while the elemental Si peak decreases to less than 5% of its original intensity (fig. 2e). By assuming a SiC layer of uniform thickness and a Si(2p) escape length of 25 Å, we estimate from fig. 2e that the SiC layer is greater than 90 Å thick. Another observation after 4.5 hours is the detection of a new type of carbon with a C(1s) peak at 284.3 eV (fig. 1e).

For longer growth periods (figs. 1f,g and 2f,g) two phenomena occur: the C(1s) peak at 284.3 eV increases in intensity concurrent with a decline in the SiC feature (282.7 eV) and the

Si intensity drops very low with no change in peak position. Figures 1f,g and 2f,g show that the surface is being covered with the new form of carbon that exhibits a C(1s) peak at 284.3 eV. The XPS survey scan after 17 hours of growth shows only a single form of carbon and a very small amount of Si. No further changes were observed by XPS after 17 hours of growth. To confirm that the C(1s) peak at 284.3 eV was due to diamond, the sample was removed from the apparatus and a Raman spectrum was obtained which exhibited the characteristic diamond line at 1332 cm^{-1}.

Conclusions

The application of XPS has for the first time elucidated some of the surface chemistry which occurs during the nucleation and growth of diamond films. We characterize the nature of the substrate prior to growth showing that the Si(100) is covered with a layer of SiO$_2$ and carbonaceous contamination. After a short period the SiO$_2$ layer and the carbonaceous contamination are removed and replaced by a layer of SiC which increases in thickness with time. Finally, diamonds nucleate and grow on the SiC layer. No other forms of carbon are observed. This experiment represents a significant improvement in the level of understanding of diamond film growth.

References

1. J.C. Angus and C.C. Hayman, *Science* 241, 913 (1988).
2. S. Matsumoto, Y. Sato, M. Kamo, N. Setaka, *Jpn. J. Appl. Phys.* 21, 183 (1982).
3. V.P. Varnin *et. al., Kristallografiya* 22, 893 (1977).
4. C.I.H. Ashby, *Appl. Phys. Lett.* 43, 609 (1983).
5. K. Kurihara, K. Sasaki, M. Kawaradi, N. Koshino, *Appl. Phys. Lett.* 52, 437 (1988).
6. S. Matsumoto, M. Hino, T. Kobayashi, *Appl. Phys. Lett.* 51, 737 (1987).
7. S.J. Harris, A.M. Weiner T.A. Perry, *Appl. Phys. Lett.* 53, 1605 (1988).
8. C.D. Wagner, W.M. Riggs, L.E. Davis, J.F. Moulder, and G.E. Muilenberg, Handbook of X-ray Photoelectron Spectroscopy (Perkin-Elmer, Eden Prairie, MN, 1979).
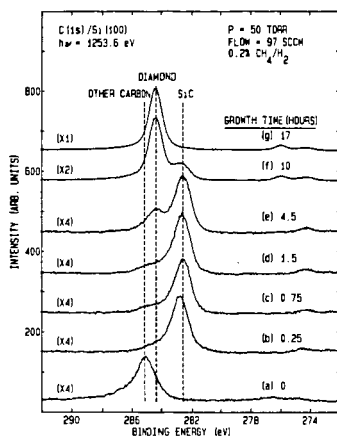9. Y. Mizokawa, T. Miyasato, S. Nakamura, K.M. Geib, and C.W. Wilmsen, *Surface Sci.* 182, 431 (1987).

Fig. 1: XPS spectra of the C(1s) region for different growth times. Data for the substrate prior to growth, t=0, show carbon contamination typical for Si cleaned with methanol prior to introduction. The other spectra, b-g, show the formation of a carbide layer (282.7 eV) followed at later times by diamond growth (284.3 eV).
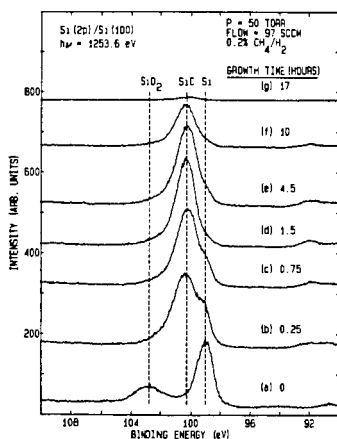

Fig. 2: XPS spectra of the Si(2p) region for different growth times. Data for the substrate at t=0, prior to growth, show that the Si(100) is covered with a thin layer of SiO₂. Data at later times show that the oxide is replaced by a carbide layer (100.3 eV) which then declines in intensity as the surface is covered with diamond.

SOME THERMODYNAMIC ASPECTS OF
CVD FILAMENT PROCESS FOR DIAMOND GROWTH

Himanshu B. Vakil
GE Corporate Research and Development
P.O. Box 8, CEB 479
Schenectady, New York 12301

INTRODUCTION

Low pressure synthesis of diamonds from hydrocarbons has seen an enormous resurgence in the last decade. After the pioneering work by Eversole in 1958 and decades of patient - but often non-reproducible - work by Deryagin and co-workers, the recent work in Japan by Matsumoto and co-workers has led to the universal acceptance of the viability of low pressure, metastable growth of crystalline diamond (ref. 1). As a result of recent work, not only has the chemical vapor decomposition (CVD) of diamonds by a simple thermal decomposition process been confirmed, but a plethora of low pressure processes have been developed - among them, plasma assisted CVD (RF, microwave, and DC), electron beam and laser assisted CVD, and deposition from ion beams, to name a few.

Despite the wide diversity of processes and operating conditions there are a few observations that have gained a near universal acceptance:

1. An abundant supply of atomic hydrogen is required at the growing diamond surface.

2. The exact chemical nature of the starting carbon source is not crucial. Almost any form of carbon source has been found satisfactory for growing diamonds. Alkanes, alkenes, alkynes, aldehydes, alcohols, and ketones have been used successfully to date.

3. Carbon concentration in the gas phase should be very low. An excessive amount leads to graphitic deposits.

4. For the thermal, filament process carbide-forming refractory metal filaments are successful in growing diamonds; carbon filaments apparently do not work. Other filaments such as platinum also do not work.

Finally, while it is generally believed that the reaction is kinetically limited, the exact rate limiting step and the growth mechanism are still topics of controversy. There have been many proposals as to which carbon specie is critical for the diamond growth with the list being made up of free radicals like $CH_3 \cdot$ and $C_2H \cdot$, gaseous carbon atoms and clusters, molecules like CH_4 or C_2H_2, and ionic species e.g., CH_3+.

The objective of this paper is to apply thermodynamic analyses to the diamond CVD process, on the one hand to give insights as to what some of the "universal" observations tell us about the process, and on the other to provide a framework for evaluating alternate hypotheses for growth mechanisms. Following a long-standing tradition at GE, our group is involved in research on a wide variety of processes for diamond synthesis, including those mentioned above. However, for the purpose of this paper, we have selected only one process - the hot filament, thermal process - primarily because it is the simplest CVD process and likely to be more amenable to thermodynamic analyses than others. In the following sections we will present results of thermodynamic equilibrium calculations aimed specifically at answering such questions as why carbon filaments do not work, or which carbon species are unlikely to be critical in diamond growth.

THERMODYNAMIC CALCULATIONS

Thermodynamics of thermal decomposition of hydrocarbons has long been a topic of interest in the context of deposition of coke or pyrolytic carbon (ref. 2). However, most of this work has dealt with atmospheric and higher pressures, and is of little direct use to the diamond CVD process. More recently, there have been a few studies aimed especially at diamond CVD (e.g., ref. 3); we hope that this paper will serve to augment such studies and provide a slightly different perspective.

Equilibrium calculations presented here were carried out using the JANAF database, with 14 gaseous species containing C and H, and one condensed specie - graphite. Diamond phase was not included since the free energy difference between graphite and diamond is quite small compared to that between gaseous species and graphite; in our opinion, the resultant simplification well justifies incurring relatively minor errors in carbon activities and gas phase specie concentrations.

Why do carbon filaments not work?

A logical place to begin an investigation of why carbon filaments apparently do not work is to examine the condensed phase activity using conditions typical of filament growth. We have selected a feed composition of 1.5 mole% methane in hydrogen at a pressure of 0.01 atmosphere (7.6 torr or 10.13 mbar) with substrate temperatures from 700C to 1100C and filament temperatures from 2000C to 2600C. Figure 1 shows the carbon activity as a function of temperature. Over the entire range of filament temperatures the condensed phase activity is below unity, thereby indicating that the gas phase is below saturation with respect to solid carbon. Conversely, substrate temperature range shows carbon activity to be significantly greater than unity, reaching a peak supersaturation of 100 in the vicinity of 1000C. This strongly suggests that it is necessary for the filament to operate with a carbon activity in the range of 0.25 to 0.9; carbide forming refractory metals meet this criterion, but carbon filaments require that the gas phase be saturated with respect to carbon.

Another way to illustrate the same point is to calculate the carbon atom fraction in the gas phase in equilibrium with solid carbon at filament temperatures. This is shown in Figure 2. In order to be in equilibrium with a carbon filament, the reactor feed needs to be as high as 28% methane at the upper end of the range, decreasing to just below 2% at a filament temperature of 2000C which may be too low to produce an adequate amount of atomic hydrogen. This would explain why the use of a carbon filament produces graphitic deposits, similar to those obtained with an excessive amount of carbon in the feed. Lower melting filaments, such as platinum, are also unsuccessful because they are unable to generate an adequate supply of atomic hydrogen.

Equilibrium distribution of hydrocarbon species

Next, let us examine the equilibrium distribution of hydrocarbon species as a function of temperature. Figure 3 is a plot of the partial pressure (in atmospheres on a logarithmic scale) over the entire temperature range for the selected case of 1.5% methane in hydrogen as a feed. Several features can be noted from the figure.

Filament region:

1.   Atomic hydrogen concentration increases rapidly from less than 10% at 2000C to over 50% at 2600C.

2. Almost all of the carbon is present as either C_2H_2 or $C_2H\cdot$, with all the other minor species accounting for roughly 0.5% of the total carbon. Only when the temperature exceeds 2500C do the species C and C_3 account for more than 1% of the carbon. The concentration of methyl radical is well below 0.1% over the entire temperature range.

Substrate region:

1. The predominant species are molecular hydrogen and methane.

2. At temperatures above 900C acetylene concentration increases gradually, overtaking methane between 1000C & 1100C - reportedly the preferred range for growing good diamond crystals. Ethylene is a distant third accounting for at best 1% of the carbon at its peak.

From these observations one is led to conclude that the role of the filament is to convert molecular hydrogen to atomic hydrogen, and to convert methane - or, for that matter, any other hydrocarbon source - to primarily acetylene and $C_2H\cdot$. The insensitivity of the process to the exact source of hydrocarbon suggests that this rearrangement proceeds fairly rapidly producing an equilibrium distribution of species, thereby obliterating any history of the feed composition. At the substrate, reverse reactions producing molecular hydrogen and methane take place, in addition, of course, to a rather slow carbon deposition reaction to form diamonds. In view of the extremely low mass transfer Peclet number in a typical filament reactor, which makes it behave more like a continuous stirred-tank reactor (CSTR), the steady-state concentrations of hydrocarbon species is determined by a balance between the source and sink rates at the filament and the substrate.

Calculated impingement rates of the various carbonaceous species using equilibrium concentrations at the filament, which provide an absolute upper bound for all species except methane and ethylene, can be compared with the observed growth rates of diamond films to obtain an estimate of the incorporation ratio (fraction of collisions resulting in film growth) required for a specific specie to be the critical one for diamond growth. Based on typical growth rates of 1 to 10 microns/hour, an average incorporation rate is approximately 4×10^{-8} g-atoms/cm^2/sec. At this growth rate, the required incorporation ratio for acetylene and $C_2H\cdot$ is roughly 1 in 1000, while that for C & C_3 is roughly 1 in 10. Since these ratios have been calculated assuming the maximum possible concentrations (equilibrium at the filament and no re-combinations thereafter), and since the substrate surface is supposedly almost totally covered with hydrogen, acetylene and $C_2H\cdot$ appear to be the most likely candidates for the critical species, with C_3 and C being less likely (but possible) ones, particularly at high filament temperatures. Other free radicals such as $CH\cdot$, $CH_2\cdot$, and particularly $CH_3\cdot$ are at too low a concentration to account for the growth rates. Methane is always a possible candidate since it can be abundant near the substrate, and ethylene can not be ruled out if one assumes complete equilibrium at the substrate. A substantial back-conversion of acetylene to methane has been experimentally observed by us based on reactor gas sample analyses, confirming the importance of the back-conversion reaction.

Simultaneous deposition of diamond and etching of graphite

It is often mentioned that one of the key elements of low pressure growth of diamonds is the ability of atomic hydrogen to etch away any graphite that may get deposited leaving behind only the diamond phase. In a process that operates in a cyclic manner (whether in time or space) there would be no inconsistencies in alternating between graphite deposition and etching conditions. In a steady-state process, however, to

maintain that bulk graphite can be deposited and then etched away would constitute a serious thermodynamic violation, since it would imply a carbon activity that was simultaneously greater than unity for deposition and less than unity for etching. If one were to invoke non-uniform temperatures on the substrate, as seen from Figure 1 parts of the substrate would have to be above 2000C for the activity to drop below unity. Experimentally, we have observed many instances where graphite is nucleated on a growing diamond film and then grows alongside the diamonds for the remainder of the experiment. This proves that once graphite is deposited during the course of diamond growth, it is there to stay unless the reactor conditions are altered.

A more difficult question to address is what happens when one uses a graphite substrate in a filament reactor: During the early stage of diamond nucleation is the graphite substrate etched? In the absence of the filament (e.g., in a furnace at 1000C) the answer would, of course, be no. Even with the filament, if the homogeneous phase were in local thermodynamic equilibrium there could be no etching. However, in the close proximity of the filament the presence of non-equilibrium concentration of atomic hydrogen makes thermodynamic arguments inapplicable. An experimental resolution of this question, while beyond the scope of this paper, is also made difficult by the fact that in the early stage of the experiment the filament is gradually coming to equilibrium with the gas by incorporating carbon, thereby significantly affecting the gas phase composition. Only a series of careful experiments can hope to resolve this very interesting question.

CONCLUSIONS

Thermodynamic equilibrium calculations were carried out for the hot filament CVD process for diamond deposition under typical conditions. It was shown that the carbon activity is considerably below unity at the filament and very high at the substrate. The failure of carbon filaments to grow diamonds was shown to be due to the gas phase in equilibrium with the filament to be excessively rich in carbon, thereby exceeding the supersaturation limits for diamond growth. Details of the gas phase concentrations were used to evaluate the likelihood of the various gas species to be critical for diamond growth.

ACKNOWLEDGEMENTS

REFERENCES

[1] R.C. DeVries, Annual Rev. Mat. Sciences, 17:161 (1987).

[2] B. Lersmacher, et. al., Carbon, vol. 5, p. 205 (1967).

[3] M. Sommer, et. al., presented at the Diamond Technology Initiative Symposium, Crystal City, VA (July, 1988).
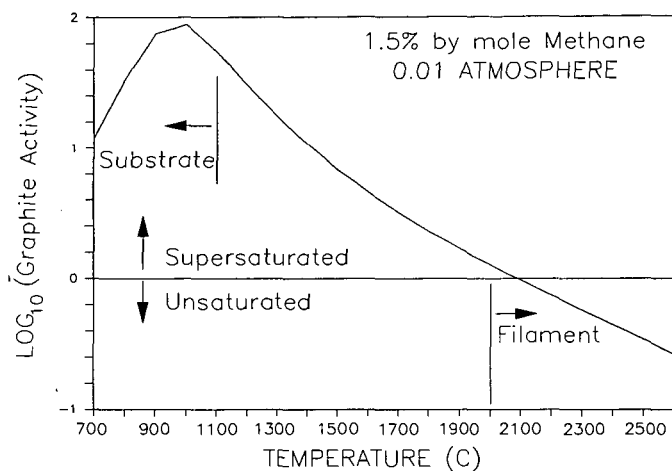
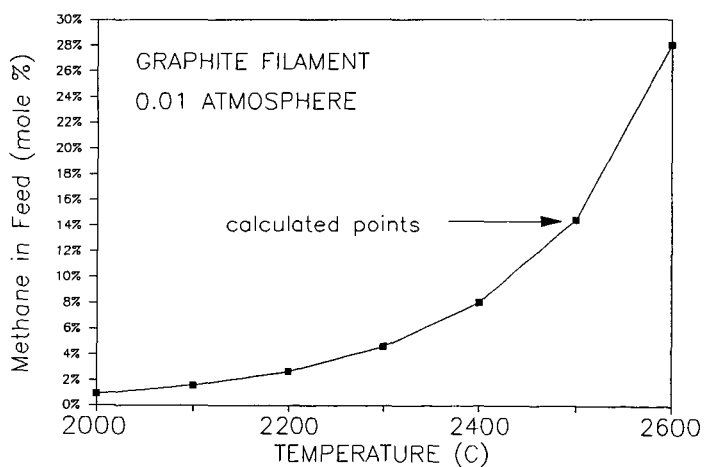Figure 1:   Graphite Activity as a function

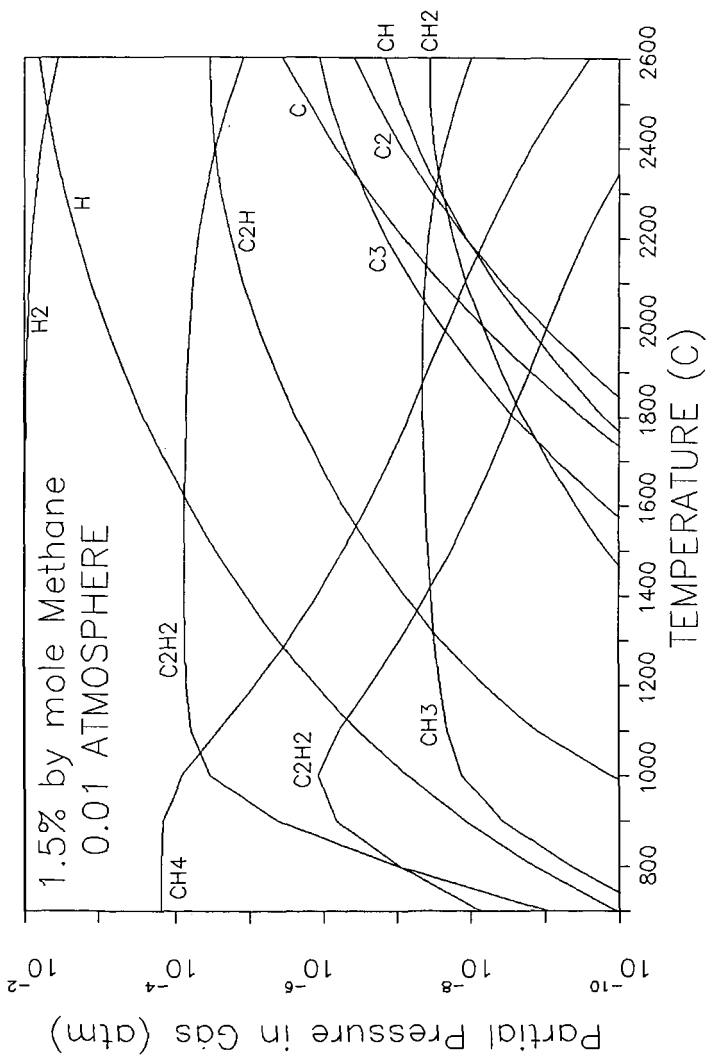Figure 2:   Feed Methane Concentration in Equilibrium
with Carbon Filament

Figure 3: Equilibrium Partial Pressures in Gas

DIAMONDS IN THE CHEMICAL PRODUCTS OF DETONATION

N. Roy Greiner
Los Alamos National Laboratory
Los Alamos, New Mexico 87545

ABSTRACT

Diamonds have been found among the solid carbonaceous chemical products of high-explosive detonations. Explosives are fuel-oxidizer systems premixed on a molecular scale. This talk discusses some aspects of the chemical and hydrodynamic environment in which these diamonds form and some characteristics of the diamonds recovered. Diamonds have been recovered from detonations of composite explosives composed of trinitrotoluene (TNT) mixed with other powdered solid explosives, such as cyclo-trimethylenetrinitramine (RDX), triaminotrinitrobenzene (TATB), ammonium nitrate (AN), and nitroguanidine (NQ). The detonations were carried out in a 1.5-m^3 tank, usually filled with 1 atm of Ar gas. Other explosive composites and one-component explosives have also been investigated. The diamonds have been characterized by transmission electron microscopy, x-ray diffraction, and various chemical means.

INTRODUCTION

Detailed knowledge of the chemical kinetics and equilibria of detonation has long been a desired, but elusive goal. One focus of this chemistry is the coagulation of carbonaceous solid (soot) from carbon initially present as the skeletal atoms of small organic molecules (typically consisting of 20 to 50 atoms). The "fuel" portion of the explosive molecule is the atoms of carbon and hydrogen, and the "oxidizer" is a number of nitro (-NO_2) groups. During detonation the fuel and oxidizer react to form water and oxides of carbon, the nitrogen forms N_2, and the carbon left over forms the soot. At least that is what is visualized. Most of what is "known" of the chemistry of detonation is an intricately convoluted mixture of supposition, computer modeling, and calibration of the models against hydrodynamic measurements of detonating material.

A brief description of the detonation process is appropriate here. The literature affords a wealth of further detail (see, for example, Refs. 1-3). The hydrodynamic aspects of the detonation process are quite well known; that is, the density (d), pressure (P), and velocity (D) of the detonation wave for particular explosives are well established. Temperature and chemical composition are obtained as secondary information derived from a hypothetical equation of state of the detonation products calibrated against d-P-D data for a set of explosives. The equation of state must account for extreme nonideality (compressibility factors of 15-25) and must contain a mixing rule for the different molecular species in the products. Knowledge of the kinetics of the detonation process is almost entirely empirical.

Our explosive charges were cylinders 50 mm dia x 100 mm long. They were initiated by a detonator-booster system on one end of the cylinder axis. The detonation wave propagates from the booster at the detonation velocity, about 8 mm/µs, as a somewhat spherical wavefront to the other end of the charge. The density of the unexploded charge is about 1.7 g/cm^3, the density in the detonation front is about 2.3 g/cm^3, and the detonation pressure is about 245 000 atm. The detonation wave traverses the length of the charge in about 12 µs. As the material detonates, the outer surface of the charge begins to expand into the external environment, in our case a large tank evacuated or filled with 1 atmosphere of Ar gas. The inner core of the detonated charge remains at a pressure near 100 000 atm for about 3 µs after passage of the detonation wave, providing a considerable time for carbon coagulation within or very near the bulk diamond stability field (Figs. 1 and 2). The most common form of the equation of state (1,4) gives a temperature of 2600 K in the steady portion of the wave and a chemical composition of H_2O, CO_2, N_2, and solid C. Chemical products recovered from quenched detonations contain many other components (3,5). There is much discussion about processes that may occur during quenching and about how to recover true detonation products (3,5).

EXPERIMENTAL

The experimental details of the detonations have been described (4). In these detonation reactions, O and N are present as well as C and H. The atomic fractions can be seen from the formulas TNT: $C_7H_5N_3O_6$, RDX: $C_3H_6N_6O_6$, TATB: $C_6H_6N_6O_6$, NQ: $CH_4N_4O_2$, and AN: NH_4NO_3. Atomic ratios are much different than those of typical chemical vapor deposition (CVD) processes. The charge compositions were made by adding solid powders to molten TNT in the following weight percentages: #27: 40 TNT/60 RDX, #36: 50 TNT/50 AN, #60: 50 TNT/50 TATB, #63: 50 TNT/50 NQ, and #10/41: 50 TNT/50 NQ. The charges were fired in a cylindrical vessel 1.5 m^3 in volume, either evacuated or filled with 1 atm of Ar gas (2,4). The soot was recovered from the vessel after the detonation of each charge. The soots were then oven dried at 105°C to constant weight.

The micromorphologies of the soots were recorded by transmission electron microscopy (TEM); the diamonds were recovered by oxidizing the soot with $HNO_3/HClO_4$ (4); the diamonds in the residue were identified by their x-ray diffraction (XRD) powder patterns, and the diameters of the recovered diamonds were determined with an x-ray diffractometer. Thermally labile components of the soot were measured with thermogravimetric analysis (TGA), and some of the components were identified with direct insertion probe mass spectrometry (DIP/MS) or gas chromatography with mass spectrometric (GC/MS) detection.

RESULTS AND DISCUSSION

TEM has shown that the soots are composed of graphite ribbons having a smallest dimension of 3-10 nm and sometimes of diamonds having diameters of 3-7 nm (4).

The interplanar spacings measured in these samples agree well with the spacings of bulk diamond.

The crude residue containing the diamonds was sometimes found by XRD to contain minor amounts of other materials such Al_2O_3, MgO, and SiO_2 knocked loose from the vessel walls. When diamonds were present, this residue amounted to 15-22 wt% of the dried soot. Diamonds were found by TEM and in the oxidation residues of samples #27, #60, and #63, but not in samples #36 and #10/41. The diameters of the diamonds in the oxidation residues were determined by the widths of their diffraction lines measured on an x-ray diffractometer, and in all three cases, they were equal to the diameter of the diamonds observed in the TEM images. The diameters determined in this manner were 7 nm in #27, 3 nm in #60 and 3 nm in #63.

No measurable residue was obtained from #10/41 (TNT/NQ), which was fired in a vacuum. This result can be compared with that of #63 (also TNT/NQ, but fired in 1 atm of Ar) where diamonds were found. Sample #10/41 underwent a process called reshock, whereby the detonation products expanding in the vacuum are shocked to a high temperature when they collide abruptly with the vessel wall. Typically this results in the reaction

$$CO_2 + C(s) \longrightarrow 2\,CO \qquad\qquad (1)$$
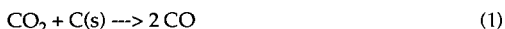
advancing far to the right because it is favored by high temperature at low density (3). Perhaps the diamonds in sample #10/41 were consumed preferentially by reaction 1. When the vessel is filled with Ar gas, much of the kinetic energy of the expanding products is absorbed by the Ar, mitigating the effects of reshock.

The residue from #36 (TNT/AN) contained only a small amount of Al_2O_3 but no diamonds. We have no explanation for this at this time.

Neither the graphite nor the diamond morphologies observed in the detonation soots seem to fit the picture of growth by aggregation. The detonation graphite appears as ribbons a few nanometers thick, not as aggregated smaller particles or crystals (4). This observation can be contrasted with the reported structures of graphitic soots from hydrocarbon flames, which are typically spheres 10-500 nm in diameter, composed of many small graphitic crystallites a few nanometers thick (6). The detonation diamonds appear to be perfect single crystals 3-7 nm in diameter and not aggregates of smaller crystals. Furthermore, the sizes of the diamond and graphite particles observed in these detonations appear to be too small for unrestricted growth by aggregation.

A model for growth of carbon solid by diffusive aggregation in the detonation product environment has been developed by Shaw and Johnson (SJ) (7). We can apply the SJ model to these detonations with the aid of a hydrodynamic model for the expansion of the detonation products. The model for the expansion also has been described (8).

Figures 1 and 2 show computed hydrodynamic histories of some representative volume elements in the charges used here. A large portion of the charge is maintained at a density near the detonation density for a time of about 3×10^{-6} s, whereas the characteristic time for aggregation in the SJ model is 2×10^{-12} s. The ratio of these two times gives the number of atoms in the most probable particle size, which is 1.5×10^6 atoms. If the most probable particle were a crystalline diamond sphere it would be 26 nm in diameter, whereas the largest particle we see is only 7 nm. By the SJ model, the volume of the most probable particle size is proportional to aggregation time, so the difference between the model and observation is large. Conversely, the size observed could be attained in only 5×10^{-9} s, if unrestricted aggregation were the limiting mechanism. The differences suggest that particle growth has additional restrictions and that aggregation progresses in increments closer in size to atoms than to small crystals.

The small size of the diamonds and the graphite ribbons raise the possibility that surface chemistry may play a role in their relative stabilities. In a spherical diamond 3 nm in diameter 37% of the carbon atoms are on the surface. If this surface were particularly stable, diamond might be more stable than graphite even without a high-pressure environment. Unfortunately, we have no direct information about the diamond or graphite surfaces in the unaltered soot. Moreover, the information we do have suggests a broad range of possibilities for the chemistry of the diamond and graphite surfaces.

Gouy-balance measurements on the raw soot show evidence of unpaired electrons, a common feature of finely divided solid carbons. Elemental analysis of the dry soots shows the presence of H, N, and O in addition to C atoms. About 1/10 to 1/20 of the atoms are N and 1/10 to 1/50 are H. TGA analysis indicates that about 30% of the soot is heat-labile (Fig. 3). Initial results from DIP and GC/MS analyses of the gases driven off of soots with moderate heat (350-400°C) show mass spectra attributable to H_2O, NH_3, CO_2, CO, HCN, HOCN, urea, alkanes, alkenes, and polycyclic aromatics often substituted with -CN and $-NH_2$ groups. DIP analysis indicates CO_2 and CO, in about a 2/1 molecular ratio, driven off a diamond residue recovered by the $HClO_4$ oxidation process. Auger/ESCA analysis of the recovered diamond residue shows the presence of N and O atoms that are removed by Ar-ion sputtering of the surface. This technique also shows that the interior of the recovered diamonds is made up of nearly pure C. These results show that the soot has a rich chemistry involving heteroatoms. The surfaces of the 3-nm diamonds contain only about 1% of the atoms in the original explosive. Given that a number of exotic chemical species have been found in the soot in quantities comparable to the number of surface atoms on the diamonds, it seems that surface chemistry of the diamonds is practically an open question.

Determining when in the hydrodynamic history (Figs. 1 and 2) the diamond growth takes place would also be of great interest.

CONCLUSIONS

Diamonds are now a well-established chemical product of the detonation process. The conditions under which they grow can be described. They appear as single crystals, not aggregates of smaller crystals, and their growth rate seems to be limited by something more than the diffusion of carbon precursors in the dense gaseous detonation products. Determination of the surface chemistry of the detonation diamonds and when in the hydrodynamic history their growth takes place remains to be done.

ACKNOWLEDGEMENTS

REFERENCES

(1) Mader, C. L., *Numerical Modeling of Detonations* (University of California Press, Berkeley, 1979).

(2) Volk, F., Bathelt, H., Schedlbauer, F., Wagner, J., *Proceedings of the Eighth Symposium (International) on Detonation*, 1985, p, 577.

(3) Ornellas, D. L., "Calorimetric Determinations of Heat and Products of Detonations for Explosives: October 1961 to April 1982," Lawrence Livermore National Laboratory report UCRL-52821, 1982.

(4) Greiner, N. R., Phillips, D. S., Johnson, J. D. , and Volk, F., *Nature*, 1988, 333, 440.

(5) Blais, N. C. and Greiner, N. R., *J. Energetic Materials* (in press).

(6) Lahaye, J. and Prado, G., in *Particulate Carbon Formation During Combustion*, D. C. Siegla and G. W. Smith, Eds. (Plenum Press, New York, 1981), p. 33.

(7) Shaw, M. S. and Johnson, J. D., *J. Appl. Phys.*, 1987, 62, 2080.

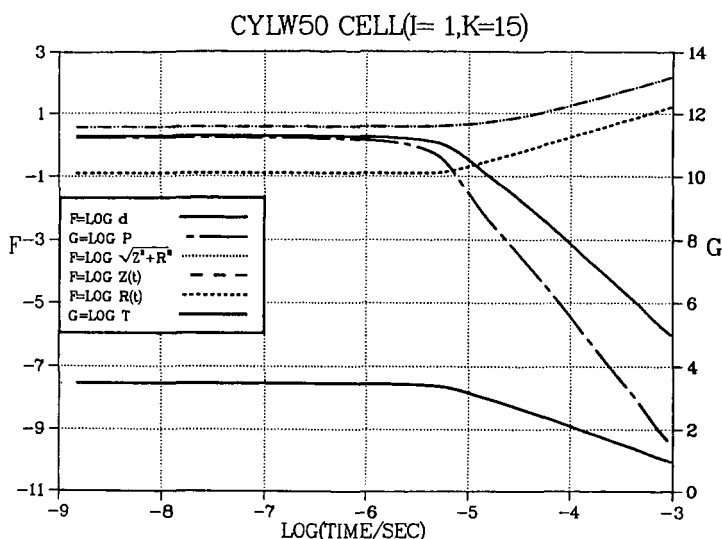(8) Greiner, N. R., *Proceedings of the 19th International Conference of ICT*, 1988, p. 36-1.

Figure 1. Hydrodynamic history of a volume element on the axis of the explosive charge 12.5 mm from the end opposite the booster charge. This volume element is representative of the detonation wave properties. The scales are logarithmic, and the units are CGS units, that is, density (d) is in g/cm^3, pressure (P) is in $dyne/cm^2$, coordinate of the volume element along the charge axis (Z) is in cm, coordinate along the charge radius (R) is in cm, and temperature derived from the equation of state (T) is in K. Log P is given on the G scale, where the value 11 represents 100 000 atm. Log P begins to depart from this value at about 3×10^{-6} s.
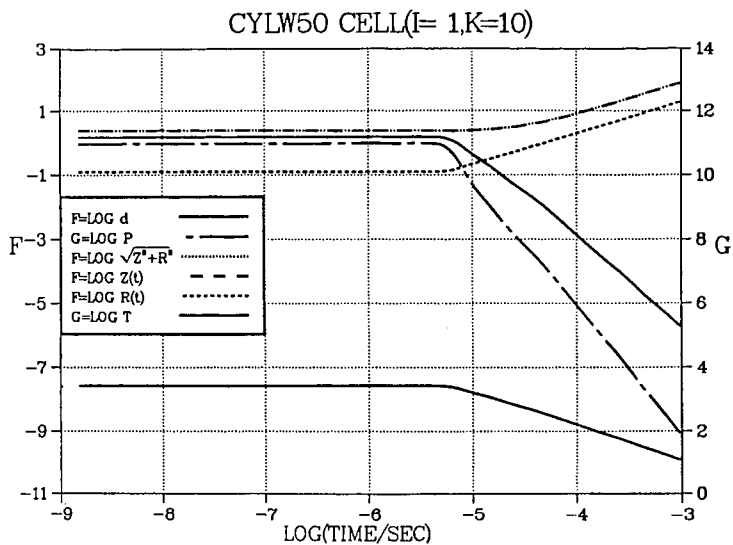
Figure 2. Hydrodynamic history of a volume element along the charge axis midway between the detonation wavefront and the booster (same scales and units as in Fig. 1). Log P is somewhat below 11 in this element, and it begins to drop below 11 after 5×10^{-6} s.
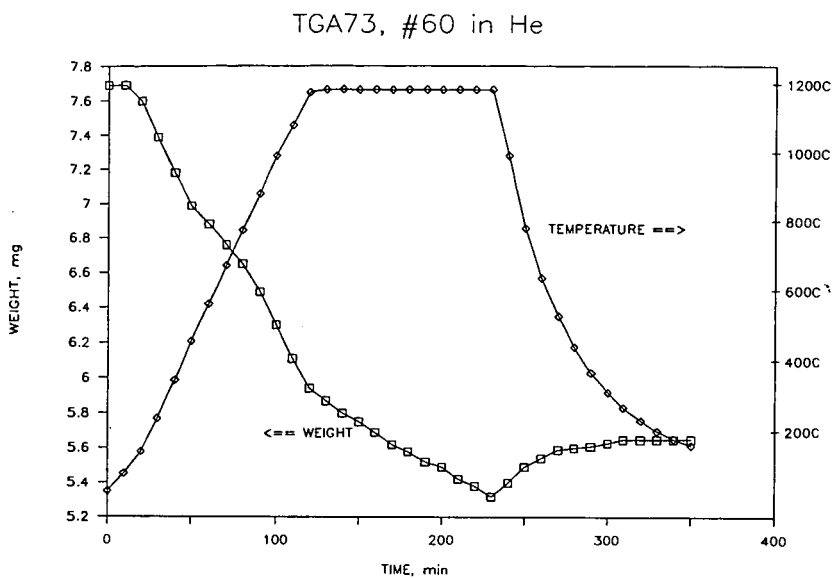
TGA73, #60 in He

Figure 3. Thermogravimetric analysis of #60 in 1 atm of He gas. There is about 10% weight loss up to 400°C, the upper limit of the evolved gas analyses, and about 25% at the termination of the run at 1200°C.

SOME EXPERIMENTS ON THE MECHANISM OF
DIAMOND FILM GROWTH

L. R. Martin and A. R. Calloway
Aerophysics Laboratory
The Aerospace Corporation, P.O. Box 92957
Los Angeles, CA 90009

INTRODUCTION

Since direct crystallization of diamond from carbon atoms is thermodynamically unfavorable at low pressures, it has been suggested by Fedoseev, et al.(1) that an "organic synthesis" picture of diamond formation is more accurate. In this picture, a diamond structure is built up by chemical reaction with carbon-containing free radicals or ions, and structure formation is controlled by kinetics rather than thermodynamics. A key problem in low pressure diamond film synthesis is the lack of a generally accepted chemical mechanism for this process. (For an example of a proposed mechanism, see Tsuda, et al.(2).) Resolution of the mechanistic question will require identification of the various chemical species present in diamond synthesis systems, and correlation of the growth rate with the concentrations of the species. A complete understanding of the mechanism can provide a rational basis for the design of improved methods for diamond synthesis.

EXPERIMENT

We have constructed a simple diamond film synthesis system with the objective of gaining mechanistic information. Our laboratory is not yet able to measure the concentrations of free radicals and ions directly, so we have designed experiments to give differing initial mixtures of free radicals. The interpretation of such experiments is complicated by the fact that rapid gas-phase chemistry takes place to change the mix of radicals, but it is possible to estimate the progress of such chemistry with kinetic modeling.

The apparatus consists of a quartz bell jar on a vacuum mainfold with provision for vacuum ultraviolet (VUV) irradiation of the substrate region as well as hot tungsten filament dissociation of the gas atmosphere. The VUV source is a hydrogen microwave discharge. The substrate material, usually single crystal silicon, was mounted on a silicon nitride heating element. The atmosphere was typically 1% organic vapor and 99% hydrogen gas at 10 torr, flowing at 100 sccm. The filament, when in use, was at 2000 Celsius and 5mm from the substrate, and the

substrate was at 850 Celsius. Experiments were done with methane, carbon monoxide, acetone, acetylene, and methyl bromide. Our assessment of the most probable initial species produced is based on thermochemistry for the tungsten filament (3) and known photochemistry for the VUV source (4).

Table 1 summarizes the experiments carried out. If we consider only neutral chemistry, our interpretation of these experiments is as follows: CH_3 and C_2H_2 are more likely to be reactants than are C, C_2H, or CH_2. This conclusion must be taken with caution because of the important influence of the gas phase chemistry. For example, a crude analysis of the reaction manifold will show that methyl radicals, CH_3, will recombine very rapidly under the conditions of the experiment, and are probably regenerated by the reaction of H-atoms with undissociated methane. This interpretation explains the apparent paradox in the table: methyl bromide is a good source of methyl radicals, yet it produces no observable diamond film. The explanation is that methyl bromide reacts rapidly with hydrogen atoms to produce a large initial concentration of methyl radicals, but these quickly recombine and leave no new source of radicals. Our experiments give no direct information about the importance of ions. In our view, ions might be generated by electron bombardment of the substrate, and therefore their possible importance cannot be ruled out in these experiments.

REFERENCES

1) D. V. Fedoseev, V. P. Varnin, and B. V. Deryagin, Russian Chemical Reviews, 53 435-444 (1984).
2) M. Tsuda, M. Nakajima, and S. Oikawa, J. Am. Chem. Soc. 108, 5780-5783 (1986).
3) J. L. Franklin, et al., Ionization Potentials, Appearance Potentials, and Heats of Formation of Gaseous Positive Ions NSRDS-NBS 26, U. S. Dept of Commerce (1969).
4) J. G. Calvert and J. N. Pitte, Jr, Photochemistry, Wiley, New York, (1966).

TABLE I

SUMMARY OF EXPERIMENTS

CARBON SOURCE	VUV	HOT WIRE	SPECIE,	RESULTS
CH_4		X	CH_3	SMALL AMOUNT OF DIAMOND
	X		CH_2	(no data)
CO		X	CO^*	DEPOSIT OF TUNGSTEN CARBIDE
	X	X	C	LONSDALEITE
$(CH_3)_2$ CO		X	CH_3	ABUNDANT DIAMOND
	X	X	CH_3	ABUNDANT DIAMOND, MORE NUCLEATION
C_2H_2		X	$C_2H_2^*$	SOME DIAMOND
	X		C_2H	SLIGHT DIAMOND, LESS THAN THERMAL
CH_3Br		X	CH_3	GRAPHITE
	X		CH_3	NO DIAMOND DEPOSIT